

See discussions, stats, and author profiles for this publication at: <https://www.researchgate.net/publication/271838047>

# Enhanced Second Harmonic Generation from an Organic Self-Assembled Eutectic Binary Mixture: A Case Study with 3-Nitrobenzoic and 3,5-Dinitrobenzoic Acids

ARTICLE *in* CRYSTAL GROWTH & DESIGN · JANUARY 2015

Impact Factor: 4.89 · DOI: 10.1021/cg5017565

---

CITATION

1

READS

85

## 8 AUTHORS, INCLUDING:



Gabin Gbabode

Normandie Université, Université de Rouen

26 PUBLICATIONS 338 CITATIONS

[SEE PROFILE](#)



Nicolas Couvrat

Université de Rouen

21 PUBLICATIONS 37 CITATIONS

[SEE PROFILE](#)



Valérie Dupray

Université de Rouen

37 PUBLICATIONS 225 CITATIONS

[SEE PROFILE](#)



Gérard Coquerel

Université de Rouen

198 PUBLICATIONS 1,533 CITATIONS

[SEE PROFILE](#)

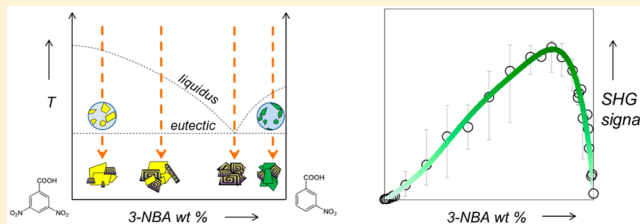
# Enhanced Second Harmonic Generation from an Organic Self-Assembled Eutectic Binary Mixture: A Case Study with 3-Nitrobenzoic and 3,5-Dinitrobenzoic Acids

Florent Simon,<sup>†</sup> Simon Clevers,<sup>†</sup> Gabin Gbabode,<sup>†</sup> Nicolas Couvrat,<sup>†</sup> Valérie Agasse-Peulon,<sup>‡</sup> Morgane Sanselme,<sup>†</sup> Valerie Dupray,<sup>\*,†</sup> and Gerard Coquerel<sup>†</sup>

<sup>†</sup>Crystal Genesis Unit, <sup>‡</sup>Chromatography Unit, Normandie Université, SMS, EA 3233 Université de Rouen, F-76821 Mont-Saint-Aignan Cedex, France

## S Supporting Information

**ABSTRACT:** This work illustrates the use of powder second harmonic generation (powder SHG), temperature-resolved second harmonic generation (TR-SHG), and second harmonic generation microscopy (SHGM) in monophasic and multiphasic sample studies. The commercial powder of 3,5-dinitrobenzoic acid was found to exhibit a significant second harmonic generation signal, whereas only two centrosymmetric polymorphic forms have been reported for this compound. Second harmonic generation techniques were used in combination with chromatography, differential scanning calorimetry, and powder X-ray diffraction to show that the SHG activity of 3,5-dinitrobenzoic acid powder originates from a chemical impurity (3-nitrobenzoic acid) present in the commercial powder under the form of a new metastable noncentrosymmetric polymorph. The metastable equilibria between 3,5-dinitrobenzoic acid and 3-nitrobenzoic acid were studied, and SHG analyses performed on crystallized binary mixtures showed significant enhancements of the SHG signal compared to that of the pure noncentrosymmetric phase. This is due to the formation of a suitable eutectic microstructure that enables quasi phase matching (QPM). In particular, powders from near-eutectic compositions exhibit SHG signals up to 20 times higher than that of the powder containing pure 3-nitrobenzoic acid noncentrosymmetric phase. This observation could provide the basis for a new route to achieve new, efficient materials for second-order frequency conversion.



## INTRODUCTION

In the field of materials science, crystallization,<sup>1–3</sup> polymorphism,<sup>4,5</sup> chemical purity, structural purity,<sup>6</sup> co-crystal screening,<sup>7</sup> and phase diagrams<sup>1,3,8</sup> are important problems for the solid-state chemist. Therefore, there is great demand for analytical methods to characterize crystalline materials. Over recent decades, while classical techniques (X-ray diffraction, differential scanning calorimetry, spectroscopy, microscopy, etc.) have been widely used for pharmaceutical materials characterization,<sup>9,10</sup> second harmonic generation (SHG)-based techniques have also been proposed for use as efficient complementary techniques. Consequently, second-order nonlinear optical materials have attracted much attention due to their high potential for photonic and optoelectronic applications (especially as frequency-doubling crystals<sup>11</sup> or devices using photonic crystals<sup>12</sup>), so SHG analysis is also relevant in systematic material analysis.<sup>13</sup>

SHG corresponds to the creation of an electromagnetic wave at twice the frequency of the incident wave. This phenomenon occurs only in noncentrosymmetric materials (i.e., without the inversion center as a symmetry element). For centrosymmetric materials, SHG cannot occur because all of the elements in the  $\chi^{(2)}$  tensor vanish.<sup>14–16</sup> Among several methods to detect the

noncentrosymmetry in crystals, SHG appears to be one of the most selective and sensitive because it allows for the detection of almost all noncentrosymmetric classes.<sup>17</sup> If noncentrosymmetric structures are not the most numerous among materials (e.g., in the Cambridge Structural Database (CSD), 24.1% of the structures reported are noncentrosymmetric),<sup>18</sup> then they are preponderant in many fields of industrial application (e.g., pharmaceuticals and optoelectronic devices), and their study is thus an important issue.

In 1968, Kurtz and Perry<sup>19</sup> developed a method for assessing the efficiency of SHG in powder samples. This method is of particular interest when suitable single crystals are not available. Powder SHG is therefore widely used for screening a high number of materials<sup>13,19–24</sup> because only a small amount of powder is required. It can also be applied to evaluate accurately the potential of new frequency-converter materials<sup>23</sup> and to assess structural<sup>25–27</sup> and chemical purity.<sup>28</sup> Moreover, powder SHG measurements are extremely fast compared to other spectroscopic methods (ca. 1 s) and very sensitive,<sup>29</sup> with a detection threshold of the noncentrosymmetric crystalline

Received: December 3, 2014

Published: January 7, 2015

phase of up to a few ppm.<sup>25</sup> For powder samples, where particles are randomly oriented, contribution to the SHG signal is the sum of the contributions from each individual particle.<sup>19</sup> The SHG signal of a given crystal mainly depends on (i) the intrinsic crystallographic features of the phase, (ii) the orientation of the crystal(s) (crystallographic axes) with reference to the fundamental beam propagation and polarization directions, (iii) the morphology of the crystals, and (iv) the crystal size distribution. This last point is important because the SHG signal is not necessarily an increasing function of the distance traveled through the crystal. With respect to SHG measurements, noncentrosymmetric crystals can be defined as either phase-matchable (PM) or not phase-matchable (NPM).<sup>16,19,30</sup> In PM materials, it can be observed under certain conditions (orientation, temperature, wavelength of the fundamental wave) that the refractive indices for both the second harmonic and fundamental waves are very close and that as a consequence the longer the distance traveled inside the crystal, the greater the SHG intensity (i.e., large particles will generate a higher SHG signal than small particles). In NPM materials, due to dispersion, these refractive indices are different, meaning that the intensity is an oscillating function of the distance traveled through the crystal with a maximal value at a particular distance called the coherence length (denoted  $l_c$ ) (and its odd multiple). The concept of phase-matching is extensively explained in the literature,<sup>14,16,30</sup> and the average coherence length, denoted  $\langle l_c \rangle$ , has been introduced for powder samples.<sup>19,21,23,31</sup>

For the study of phases transitions, powder SHG can also be coupled with a heating stage (temperature-resolved SHG or TR-SHG).<sup>13,25</sup> This has been used in several works to date, with application to monotropic,<sup>26</sup> enantiotropic,<sup>29,32–34</sup> and order-disorder<sup>35</sup> phase transitions. It should be noted that the evolution of the SHG signal with pressure was also recently studied.<sup>31</sup>

For particle imaging, SHG microscopy (SHGM) allows 2D or 3D views of noncentrosymmetric zones (e.g., crystals, domains, defects) inside a bulk sample. SHGM has proven to be of great relevance for imaging in several fields such as biology<sup>36</sup> or materials science.<sup>37</sup> For example, SHGM was used to monitor the crystallization of a noncentrosymmetric phase from a supersaturated solution *in situ*,<sup>38</sup> to selectively detect the presence of an active pharmaceutical ingredient inside an excipient matrix,<sup>39</sup> to investigate microstructure,<sup>40–42</sup> to image a crystal undergoing a polymorphic transition,<sup>26</sup> or to help the characterization of metastable polymorphs.<sup>43</sup> Recently, newly designed apparatus are capable of image acquisition at video rates.<sup>44</sup> For crystallographic purposes, polarization-controlled SHGM has been applied to crystallographic point group determination of noncentrosymmetric powder samples.<sup>45,46</sup>

Herein, SHG-based techniques are applied to study the polymorphic systems of 3,5-dinitrobenzoic acid (DNBA) and 3-nitrobenzoic acid (3-NBA), two organic compounds, and their phase equilibria. During co-crystal screening, the commercial powder of DNBA was found to exhibit a SHG signal at ambient temperature. As DNBA is known to crystallize in two polymorphic forms whose crystalline structures are both centrosymmetric,<sup>47</sup> this result revealed *a priori* a contradiction between the space group assignment and the SHG activity of the sample. This led us to characterize the polymorphism of DNBA. In this article, we describe our investigations on the origin of the SHG signal observed in a commercial powder of DNBA, which is due to the presence of a new metastable

polymorph of the contaminant, 3-NBA, and we demonstrate that SHG techniques could also be of great interest to assess chemical purity even when the identified contaminant exhibits polymorphism and metastability. The binary phase diagram between DNBA and 3-NBA is also studied. We report high SHG efficiencies for a crystallized binary mixture of DNBA and 3-NBA at some characteristic compositions. This result is correlated with the particular microstructures arising from eutectic-forming systems, which lead to a quasi-phase-matching (QPM) mechanism.

## MATERIALS AND METHODS

**Materials.** 3,5-Dinitrobenzoic acid (CAS registry number 99-34-3, molar mass 212.12) and 3-nitrobenzoic acid (CAS registry number 121-92-6, molar mass 167.12) were purchased from Alfa Aesar with a chemical purity higher than 98%. The different samples used for this study are as follows:

*ComDNBA* and *Com3-NBA*. Commercial DNBA and 3-NBA, respectively, without further treatments.

*RecDNBA* and *Rec3-NBA*. Crystallized powders obtained by total evaporation at ambient temperature in opened crystallizers of undersaturated solutions of *ComDNBA* and *Com3-NBA*, respectively, in usual solvents (acetone, water, methanol, ethanol, butanol, acetonitrile, hexane, and mixtures). The first crystals appeared between 2 and 6 h.

*FusDNBA* and *Fus3-NBA*. Samples crystallized from the melt of *ComDNBA* and *Com3-NBA*, respectively, at high temperature (ca. 10 °C above the melting points, 220 and 150 °C, respectively).

Single crystals of DNBA were grown by slow evaporation in organic solvents in order to obtain suitable samples for single-crystal X-ray diffraction measurements and optical microscopy.

To draw the metastable solid–liquid equilibria between DNBA and 3-NBA, *ComDNBA* and *Com3-NBA* powder mixtures were prepared at various compositions and were completely dissolved in acetone in 9 mL glass vials. Then, the resulting solutions were left to crystallize by solvent evaporation at room temperature. For each crystallized powder mixture, the phases were analyzed with XRPD, DSC, and SHG.

The solid–liquid stable equilibria between DNBA and 3-NBA were also studied by analyzing milled powder mixtures prepared from *ComDNBA* and *Com3-NBA* powders. Milled samples were obtained using a Retsch Mixer Mill MM 200, with radial oscillations in a horizontal position set at 25 Hz for 20 min at room temperature.

**X-ray Powder Diffraction (XRPD).** X-ray powder diffraction analyses were carried out on a D8 Discover system (Bruker). The instrument is equipped with an X-ray tube containing a copper anode, (40 kV, 40 mA,  $K\alpha_1$  radiation = 1.5406 Å,  $K\alpha_2$  radiation = 1.5444 Å) and is mounted with an angular detector, Lynx eye. The scan step was fixed at ~0.04° with a counting time of 0.5 s/step over an angular range 3–30° in  $2\theta$ . The system is monitored with Diffract. plus XRD commander software, version 2.6.1.

**Temperature-Resolved X-ray Powder Diffraction (TR-XRPD).** Crystalline solid phases were analyzed by means of X-ray powder diffraction (XRPD) on a Bruker Siemens D5005 apparatus ( $\theta-\theta$ ) set, with  $Cu K\alpha_1$  radiation (1.54056 Å) ( $K\beta$  filter) under 40 kV and 30 mA and collected on a scintillation detector. The  $\theta$  angle calibrations were carried out using Siemens slits and a quartz sample (secondary standard). Temperature was controlled and monitored using an Anton Paar TTK450. The intensity was measured with a  $2\theta$  step of 0.04° during 4 s.

**Single-Crystal X-ray Diffraction (SC-XRD).** Single crystals were stuck on glass fibers and mounted on the full three-circle goniometer of a Bruker SMART APEX diffractometer ( $Mo K\alpha$ ,  $\lambda$  = 0.71073 Å) with a CCD area detector. Three sets of exposures (1800 frames) were recorded, corresponding to three  $\omega$  scans, for three different values of  $\varphi$ . The cell parameters and the orientation matrix of the crystal were preliminary determined by using SMART software.<sup>7</sup> Data integration and global cell refinement were performed with SAINT software.<sup>8</sup> Intensities were corrected for Lorentz, polarization, decay, and

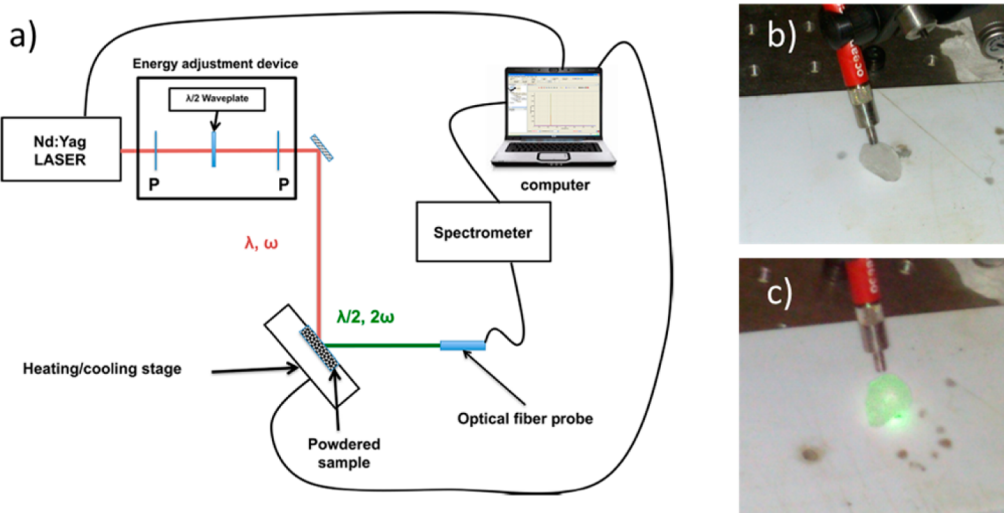


**Figure 1.** (a) Experimental setup of powder SHG composed of an Nd:YAG Q-switched laser operating at a frequency of 1064 nm; (b) KDP crystal before irradiation with the Nd:YAG laser; and (c) KDP crystal irradiated with the Nd:YAG laser showing second harmonic generation (the crystal emitted green light (frequency at 532 nm), which consisted of the conversion of the fundamental beam).

absorption effects and reduced to  $F_o^2$ . The program package SHELXTL<sup>9</sup> was used for space group determination, structure solution, and refinement. The space group was reliably determined from systematic extinctions and relative  $F_o^2$  of equivalent reflections (XPREP). The structure was solved by direct methods (SHELXS). Analysis was performed at two temperatures: 200 and 300 K.

**Differential Scanning Calorimetry (DSC).** Thermal analyses of the solids were conducted on DSC 204 F1 Netzsch equipped with an Intracooler. Solid samples (mass of ca. 3–15 mg) were placed in a 25  $\mu\text{L}$  closed aluminum crucible. The atmosphere of the analyses was regulated by Helium flux (40  $\text{mL min}^{-1}$ ), and heat runs were conducted at different heating rates. The data treatment was performed with Netzsch-TA Proteus software, v4.8.4.

**Second Harmonic Generation (SHG) and Temperature-Resolved Second Harmonic Generation (TR-SHG).** A Nd:YAG Q-switched laser (QuanTEL) operating at 1.06  $\mu\text{m}$  was used to deliver 360 mJ pulses of 5 ns duration with a repetition rate of 10 Hz. An energy adjustment device made up of two polarizers (P) and a half-wave plate ( $\lambda/2$ ) allowed the incident energy to be varied from 0 to ca. 200 mJ per pulse. An RG1000 filter was used after the energy adjustment device to remove light from the laser flash lamps. For TR-SHG, the samples (a few milligrams of powder in a crucible) were placed in a computer controlled heating–cooling stage (Linkam THMS-600) and were irradiated with a beam (diameter of 4 mm). The heating stage can be removed for measurements at ambient temperature. The setup is shown in Figure 1. The signal generated by the sample (diffused light) was collected into an optical fiber (500  $\mu\text{m}$  of core diameter) and directed onto the entrance slit of a spectrometer (Ocean Optics). A boxcar integrator allowed an average spectrum (spectral range 490–590 nm) with a resolution of 0.1 nm to be recorded over 2 s (20 pulses). To avoid problems related to sublimation of the samples, the heating stage was opened, but only during the SHG measurements, so it had no significant influence on temperature regulation. According to Kurtz and Perry's SHG powder method,<sup>19</sup> the SHG signal intensities of the samples were compared to the signal of a reference compound ( $\alpha$ -quartz, 45  $\mu\text{m}$  average size). In order to qualitatively compare the samples among each other, an equivalent mass of each solid was used for every analysis (ca. 200 mg).

**Second Harmonic Generation Microscopy (SHG Microscopy).** A laser scanning microscope LSM 710 NLO Zeiss (Ina, Germany) was used for DNBA powder observations. Excitation was provided by a CHAMELEON femtosecond titanium-sapphire laser (Coherent, Santa Clara, CA, USA) set at 860 nm. Samples were deposited in glass bottomed bow and were imaged with a 20 $\times$ , 0.8 NA oil objective lens. The SHG signal emitted was collected with a

bandpass filter (420–440 nm). Z-stacks images were acquired with a 0.8  $\mu\text{m}$  Z step.

**Optical Microscopy.** Optical microscopy observation was conducted by a Nikon SMZ-10A (Nikon Imaging Ltd.) coupled to a CCD camera connected to a computer.

**Scanning Electron Microscopy (SEM).** Scanning electron microscopy (SEM) pictures were obtained with a JEOL JCM-5000 NeoScope instrument (secondary scattering electron) at an accelerating voltage between 10 and 15 kV. Samples were stuck on a SEM stub with gloss carbon and coated with gold, to reduce electric charges induced during analysis, with a NeoCoater MP-19020NCTR.

**Ionic/Semipreparative Chromatography.** Semipreparative HPLC was performed using a ThermoElectron system equipped with a PC1000 pump and a Spectra Physics UV 100 detector. A Hypersil Gold column (250 mm  $\times$  21.2 mm i.d., 5  $\mu\text{m}$ ) was used. The detection wavelength was set at 254 nm, and the flow rate was fixed at 8  $\text{mL min}^{-1}$ . The mobile phase consisted of an isocratic binary mixture (70:30 v/v) of EtOH/H<sub>2</sub>O containing 0.1% trifluoroacetic acid. The injection volume was 1 mL. 50 mg of DNBA in 200 mL of a mixture of EtOH/H<sub>2</sub>O (50:50 v/v) was purified by semipreparative HPLC. The fraction corresponding to the peak at a retention time of 40 min was collected and then evaporated to dryness. Ten injections were necessary to yield 50 mg of DNBA. According to the resolution ( $R \geq 2$ ), DNBA is collected with a purity of 99%. A Dionex ICS-3000 was used in this work that included a pump degasser, a column heater, an AS40 autosampler, and Chromeleon workstation. Analysis was carried out on an OMNIPAC PCX-100 analytical column (250 mm  $\times$  4 mm) working at a flow rate of 1  $\text{mL min}^{-1}$ . The detection wavelength was set at 254 nm (Ultimate 300 RS). The injection volume was 20  $\mu\text{L}$ . The mobile phase was a mixture of an aqueous solution (4 mM NaOH, 1 M NaCl) (A), acetonitrile (B), and water (C). The gradient was composed of 20:20:40 (v/v/v) at the initial step toward 50:20:30 after 20 min. The retention time of DNBA is 2.88 min.

## RESULTS AND DISCUSSION

**Polymorphism of 3,5-Dinitrobenzoic Acid (DNBA).** Crystallized samples of DNBA were prepared by a solvent-evaporation method in acetone (RecDNBA) and from the molten state (FusDNBA) and were analyzed by XRPD, DSC, and powder SHG. DNBA was reported to crystallize in two centrosymmetric polymorphic forms (referenced in the Cambridge Structural Database (CSD) as C2/c, CUCKAM02, and P2<sub>1</sub>/c, CUCKAM01).<sup>47</sup> Due to their apparent enantiotropic relationship, they are referenced throughout as DNBA<sub>LT</sub> (low-

temperature form, CUCKAM02) and 3-NBA<sub>HT</sub> (high-temperature form, CUCKAM01), respectively.

XRPD analyses were performed on *Com*DNBA, *Rec*DNBA, and *Fus*DNBA in the  $2\theta$  range from  $3^\circ$  to  $30^\circ$  at room temperature (Figure 2). The X-ray diffraction patterns of

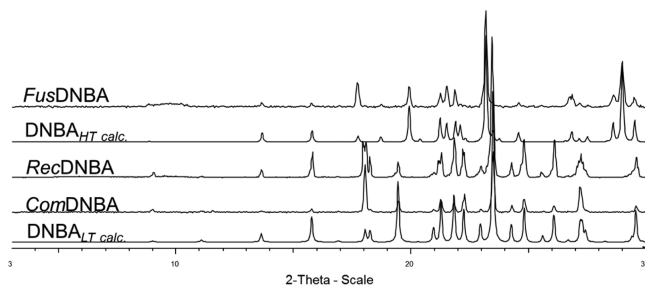


**Figure 2.** XRPD patterns in the  $2\theta$  range from  $3^\circ$  to  $30^\circ$  for *Com*DNBA, *Rec*DNBA, and *Fus*DNBA and calculated XRPD patterns from the CSD for DNBA<sub>LT</sub> and DNBA<sub>HT</sub>.

*Com*DNBA and *Rec*DNBA match the X-ray diffraction pattern of the centrosymmetric polymorph calculated from the CSD data ( $C_2/c$  CUCKAM02,<sup>47</sup> labeled DNBA<sub>LT,calc</sub>). The X-ray diffraction patterns of *Fus*DNBA fits that of the second centrosymmetric polymorph ( $P_{2_1}/c$  CUCKAM01,<sup>47</sup> labeled DNBA<sub>HT,calc</sub>).

DSC analyses were performed on *Com*DNBA, *Rec*DNBA, and *Fus*DNBA with a  $5\text{ K min}^{-1}$  heating rate (Figure 3). Two

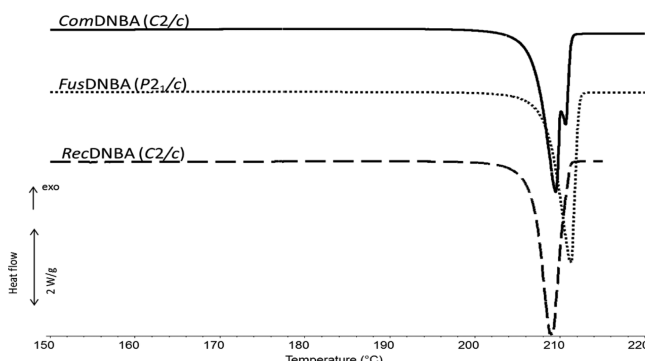


**Figure 3.** Thermograms from  $170$  to  $230\text{ }^\circ\text{C}$  for *Com*DNBA (solid line), *Rec*DNBA (dotted line), and *Fus*DNBA (dashed line) (heating rate of  $5\text{ K min}^{-1}$ ).

endothemic peaks between  $200$  and  $208\text{ }^\circ\text{C}$  are observed for *Com*DNBA and *Rec*DNBA. These two peaks can be described as the fusion of DNBA<sub>LT</sub> followed by the fusion of DNBA<sub>HT</sub>. Despite the heating rate of  $5\text{ K min}^{-1}$ , chosen in order to obtain the better separation of the peaks, the events are too close to allow a precise determination of the fusion temperature of DNBA<sub>LT</sub> and to observe the recrystallization of DNBA<sub>HT</sub>. For *Fus*DNBA, a single thermal event, corresponding to the fusion of the high-temperature polymorph, is observed. The onset fusion temperature is  $208.4\text{ }^\circ\text{C}$ , with a melting enthalpy of  $31.28\text{ kJ mol}^{-1}$  and melting entropy of  $64.96\text{ J mol}^{-1}\text{ K}^{-1}$ . Therefore, according to these DSC results, the relationship between the two polymorphs seems to be of enantiotropic character.

Powder SHG measurements performed on the different samples showed that *Com*DNBA and *Rec*DNBA samples exhibit SHG activity between  $0.5$  to  $20\%$  of the reference  $\alpha$ -

quartz signal, depending on the sample characteristics (e.g., crystal size distribution, solvent from which DNBA had been crystallized). Note that DNBA was already reported to exhibit a small SHG activity ( $1.5\%$  of the reference  $\alpha$ -quartz signal),<sup>20</sup> without further comments. *Fus*DNBA samples did not generate any detectable SHG signal.

#### Polymorphism of 3-Nitrobenzoic Acid (3-NBA).

Crystallized samples of 3-NBA were prepared by solvent evaporation (*Rec*3-NBA) and from the molten state (*Fus*3-NBA) with the commercial product (*Com*3-NBA) and were analyzed by XRPD, DSC, and powder SHG. 3-NBA was reported to crystallize in two centrosymmetric polymorphic forms (referenced in the CSD database as  $P_{2_1}/c$ , MNBZAC04 (or MNBZAC), and  $P_{2_1}/c$ , MNBZAC01).<sup>48,49</sup> Due to their apparent enantiotropic relationship, they are hereafter referred to as 3-NBA<sub>LT</sub> (low-temperature form, MNBZAC04) and 3-NBA<sub>HT</sub> (high-temperature form, MNBZAC01).

XRPD analyses were performed on *Com*3-NBA, *Rec*3-NBA, and *Fus*3-NBA in the  $2\theta$  range from  $3^\circ$  to  $30^\circ$  at room temperature (Figure 4). The X-ray diffraction pattern of *Com*3-

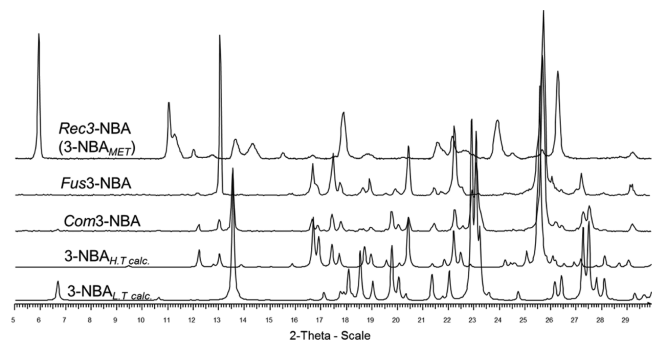


**Figure 4.** XRPD patterns in the  $2\theta$  range from  $3^\circ$  to  $30^\circ$  for *Com*3-NBA, *Rec*3-NBA, and *Fus*3-NBA and calculated XRPD patterns from the CCSD for 3-NBA<sub>LT</sub> and 3-NBA<sub>HT</sub>.

NBA matches the X-ray diffraction pattern of the centrosymmetric polymorph calculated from the CSD data ( $P_{2_1}/c$ , MNBZAC04,<sup>48</sup> labeled 3-NBA<sub>LT,calc</sub>). The X-ray diffraction patterns of *Fus*3-NBA fits the X-ray diffraction patterns of the second centrosymmetric polymorph ( $P_{2_1}/c$  MNBZAC01,<sup>49</sup> labeled 3-NBA<sub>HT,calc</sub>). The X-ray diffraction pattern of *Rec*3-NBA does not correspond to either of the two polymorphs. Thus, *Rec*3-NBA constitutes a new phase that has not been already reported (hereafter labeled 3-NBA<sub>MET</sub>).

Powder SHG measurements performed on *Rec*3-NBA samples showed that this compound exhibits SHG activity between ca.  $30$  and  $200\%$  of the reference  $\alpha$ -quartz signal. Powder of 3-NBA<sub>MET</sub> was sieved over different particle size ranges in order to characterize the material with regard to its phase matchability for SHG (Figure 5).

Results show that 3-NBA<sub>MET</sub> is not phase-matchable (NPM) for SHG. Therefore, the SHG signal is an oscillatory function of the particle size. Note that a lower evaporation rate (e.g., closed vs open crystallizer) could lead to the formation of 3-NBA<sub>LT</sub>. It can be easily detected experimentally by the fact that 3-NBA<sub>LT</sub> material was present as yellowish transparent crystals, whereas 3-NBA<sub>MET</sub> material was present as off-white agglomerated thicker crystals. Contrary to that for *Rec*3-NBA, *Fus*3-NBA samples did not generate any detectable SHG. *Com*3-NBA samples also exhibited no SHG, but *Com*3-NBA from other commercial providers was sometimes found to be SHG-positive

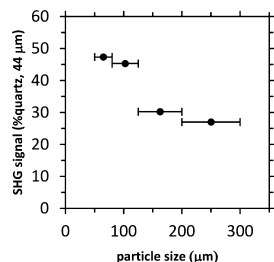


**Figure 5.** SHG signal vs particle size range of the different sieved fractions. 3-NBA<sub>MET</sub> was found to be not phase-matchable (NPM) for SHG. No preponderant polymorphic transition toward 3-NBA<sub>LT</sub> occurred during sieving.

(ca. 0.5–2% of the  $\alpha$ -quartz reference signal), which can be understood by the presence of 3-NBA<sub>MET</sub> as a structural impurity.

The high SHG activity of this new polymorph (3-NBA<sub>MET</sub>) is a good indicator of a noncentrosymmetric structure. Unfortunately, single crystals of this new form could not be isolated from solution since the slow crystallization leads to the 3-NBA<sub>LT</sub> form. Several attempts to solve the crystal structure of 3-NBA<sub>MET</sub> from X-ray powder diffraction data of moderate (conventional laboratory X-ray source) to high (synchrotron source) resolution were undertaken. However, suitable unit cell dimensions could not be found, especially due to the large peak width usually observed (regardless of the data set), which indicated significant uncertainties regarding the peak positions. A possible explanation may be a strong Scherrer effect due to the small crystallite size of the recrystallized powder. Other crystallization methods that lead to the formation of 3-NBA<sub>MET</sub> were tried, such as sublimation or precipitation from an antisolvent, but no XRPD patterns of better quality could be recorded. Another alternative to obtain symmetry information in a future attempt could be the use of polarized SHGM,<sup>45,46</sup> which allows point group determination in random powder samples, provided that small single crystals can be visually isolated.

DSC analyses were performed on *Com*3-NBA, *Rec*3-NBA, and *Fus*3-NBA (Figure 6) to establish the relative stability of

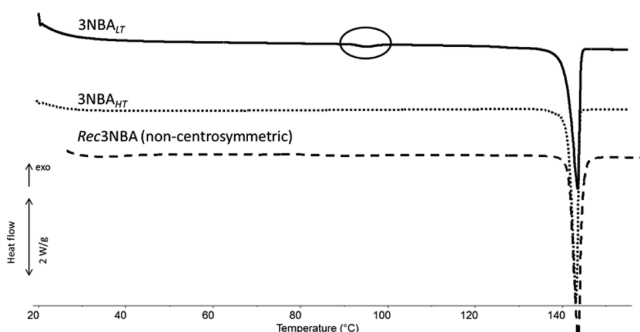


**Figure 6.** Thermograms from 20 to 150 °C for 3-NBA<sub>LT</sub> (solid line), 3-NBA<sub>HT</sub> (dotted line), and Rec3-NBA (dashed line) (heating rate of 5 K min<sup>-1</sup>).

the three polymorphs. The results show enantiotropic phase behavior between the two stable polymorphs (with the polymorphic transition determined at 92.2 °C (onset) between the low-temperature form (3-NBA<sub>LT</sub>) and the high-temperature form (3-NBA<sub>HT</sub>). The melting point of 3-NBA<sub>HT</sub> was determined to be 141.0 °C (onset).

The new polymorph (3-NBA<sub>MET</sub>) was found to be metastable at all temperatures examined. It presents the same melting point as 3-NBA<sub>HT</sub>, suggesting that the polymorphic transition toward the stable form occurred upon heating. The thermal phenomenon related to this monotropic transition was not clearly visible in the DSC curve, but TR-SHG experiments performed at the same heating rate (Figure 7) showed a

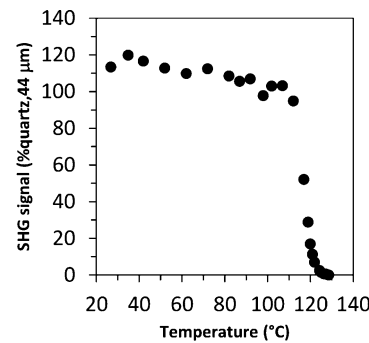


**Figure 7.** TR-SHG on a 3-NBA<sub>MET</sub> powder sample from 25 to 127 °C (heating rate of 5 K min<sup>-1</sup>).

decrease in the SHG signal at ca. 100 °C. The melting enthalpy of the 3-NBA<sub>HT</sub> polymorph was calculated to be 17.06 kJ mol<sup>-1</sup> and the melting entropy, 41.29 J mol<sup>-1</sup> K<sup>-1</sup>, from DSC data.

In order to ensure that a given sample of 3-NBA<sub>MET</sub> remains structurally pure over time and with changes in temperature, different annealing and grinding experiments were carried out.

**Kinetic Stability of 3-NBA<sub>MET</sub>.** A monotropic phase transition toward the stable low-temperature form was observed at ambient temperature after a period varying between few days and several weeks, depending on the preparation of the sample (i.e., whether a low content of the other polymorphs was present), the quantity of matter, and the storage conditions. 3-NBA<sub>MET</sub> was observed to be rather stable when stored at a temperature below 50 °C (apparition of only a small amount of the stable polymorph was determined by XRPD). However, 3-NBA<sub>MET</sub> was observed to be sensitive to transportation and very sensitive to mechanical stress. Cross-seeding experiments (i.e., suspension containing 3-NBA<sub>LT</sub> and 3-NBA<sub>MET</sub> in classical solvents) also led to the rapid conversion of the 3-NBA<sub>MET</sub> polymorph toward the stable 3-NBA<sub>LT</sub> polymorph (detected by XRPD experiments), but a small SHG signal was still observed (ca. 1–2% of the reference  $\alpha$ -quartz signal), which may correspond to the formation of 3-NBA<sub>MET</sub> during filtration due to the evaporation of the remaining solvent.

**Origin of the SHG Activity of DNBA.** Table 1 summarizes the main characteristics of the various DNBA and 3-NBA samples in terms of XRPD and SHG analyses.

It appears clearly that the SHG activity of *Com*DNBA or *Rec*DNBA powder is not consistent with the space group assignment (i.e., the structures of the two polymorphs are centrosymmetric and thus they should not exhibit SHG). The presence of a new, noncentrosymmetric polymorphic form of DNBA in the samples was not established along the exploration of the polymorphic landscape of DNBA, and SHG activity was observed only for DNBA<sub>LT</sub>, which is associated with space group C2/c. In order to resolve this apparent ambiguity, several hypotheses concerning the possible source of noncentrosymmetry were considered: (i) a wrong assignment of the structure, (ii) a laser-induced polymorphic transition from DNBA<sub>LT</sub>

**Table 1.** Polymorphic Forms, Corresponding CSD Reference XRD Patterns, Space Groups, and SHG Activities of the Different Samples Prepared throughout This Study

sample	polymorphic form	corresponding CSD reference code	reported space group	SHG activity (in % of the $\alpha$ -quartz signal)
ComDNBA	DNBA <sub>LT</sub>	CUCKAM02	C2/c	low (0.5–20%)
RecDNBA	DNBA <sub>LT</sub>	CUCKAM02	C2/c	low (0.5–20%)
FusDNBA	DNBA <sub>HT</sub>	CUCKAM01	P2 <sub>1</sub> /c	null
Com3-NBA	3-NBA <sub>LT</sub>	MNBZAC04	P2 <sub>1</sub> /c	null or low (0.5–2%)
Rec3-NBA	3-NBA <sub>MET</sub> (new)	not referenced	unknown	strong (30–200%)
Fus3-NBA	3-NBA <sub>HT</sub>	MNBZAC01	P2 <sub>1</sub> /c	null

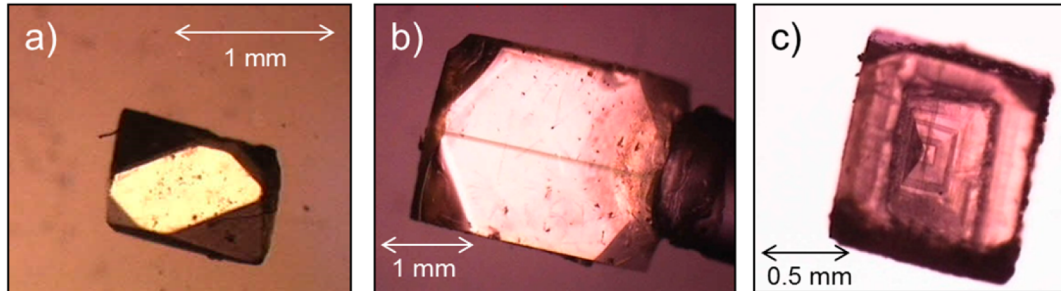


**Figure 8.** (a) Crystal without macroscopic defects, (b) crystal exhibiting twinning, and (c) crystal exhibiting a hopper face.

toward a noncentrosymmetric new polymorphic form, (iii) the presence of defects (which create zones of noncentrosymmetry by the formation of multiple interfaces) inside the crystals (with a sufficient periodic repetition in order to generate SHG), and (iv) the presence of at least one noncentrosymmetric impurity.

(i) A wrong assignment of the crystal structure<sup>50</sup> or a partial disorder at the solid state<sup>51</sup> can constitute a slight deviation from the centrosymmetry, reducing the overall symmetry to a noncentrosymmetric structure. This hypothesis was investigated for the DNBA<sub>LT</sub> form. Admittedly, it is possible (from SC-XRD results) to solve the crystalline structure of DNBA<sub>LT</sub> in the noncentrosymmetric Cc group instead of the C2/c space group (see the Supporting Information). With this hypothesis, the noncentrosymmetry could be explained by the possible partial disorder on at least one molecule of the asymmetric unit, removing the inversion center. Interestingly a slightly better reliability factor is obtained for the solution in the Cc space group. However, it can be deduced from the refinement parameters that the C2/c and Cc structures are equivalent in terms of their existence probability because the number of parameters is not the same for the resolution in both space groups. Moreover, the resolving software Platon gave a preference to the centrosymmetric C2/c structure. Furthermore, it is well-known that the Cc space group has often been corrected for many crystal structures.<sup>50</sup> In addition, the structures of DNBA polymorphs have been recently carefully investigated by neutron diffraction and SC-XRD at low temperatures and room temperature (300 K) by Jones et al., and these authors confirmed the centrosymmetric structure assignment.<sup>52</sup> Space group C2/c is thus the most probable description for the apparent symmetry of the single crystal analyzed. The possibility of SHG induced by H-bond disorder can also be rejected. It was reported that both polymorphs of DNBA exhibit H-bond disorder.<sup>52</sup> However, this is manifest still within the centrosymmetric space groups, so the possibility of any SHG signal induced by this H-bond disorder was discarded.

(ii) If laser-induced transformation was reported earlier for a charge-transfer material with a paraelectric-to-ferroelectric

structural change,<sup>53</sup> then the authors used a higher energy laser (femtosecond laser) and a material where electronic and structural changes were strongly coupled (the material consists of a mixed stack of electron-donor and -acceptor molecules).<sup>53</sup> On the contrary, DNBA contains only electron-acceptor-type groups. Consequently, this hypothesis was ruled out in this occurrence.

(iii) Optical microscopy and scanning electron microscopy (SEM) experiments were carried out on large crystals grown from an undersaturated solution of commercial DNBA to observe possible defects. No particular correlation was found between the crystal faces and the solvent of crystallization. Some crystals present no preponderant macroscopic defects (Figure 8a), whereas others exhibit twinning (Figure 8b), and, more interestingly, some crystals present an inverted pyramid defect (Figure 8c). Such defects were reported as hopper face.<sup>54</sup> This defect takes place on the face stacked to the crystallizer surface because crystals edges and corners grow faster than their faces for crystals grown at high supersaturation without stirring.<sup>55–57</sup> Whatever the solvent or the mixture of solvents used, DNBA crystals were found to crystallize in the C2/c structure (DNBA<sub>LT</sub>), as confirmed by XRPD analyses. Concerning the SHG signal, no correlation was found between the presence of defects (hopper-type crystals and twinned crystals) and the intensity of the SHG signal. Thus, the aforementioned defects are important in size and have no sufficient repetition in the bulk structure of the crystals to generate any detectable SHG.

(iv) The last hypothesis checked was the presence of impurities. These can be either structural<sup>25,26</sup> or chemical. The mechanism by which impurities induce SHG can be different in nature (e.g., formation of a noncentrosymmetric salt between DNBA and an impurity cation, formation of a noncentrosymmetric defined compound between DNBA and its impurity, crystalline impurities generating SHG by themselves, or formation of a noncentrosymmetric solid solution where impurities stack on special site of the crystal, lowering the overall symmetry of the entire crystal).<sup>58</sup> If noncentrosymmetric salts<sup>59</sup> or co-crystals<sup>60</sup> of 3,5-dinitrobenzoic acid were

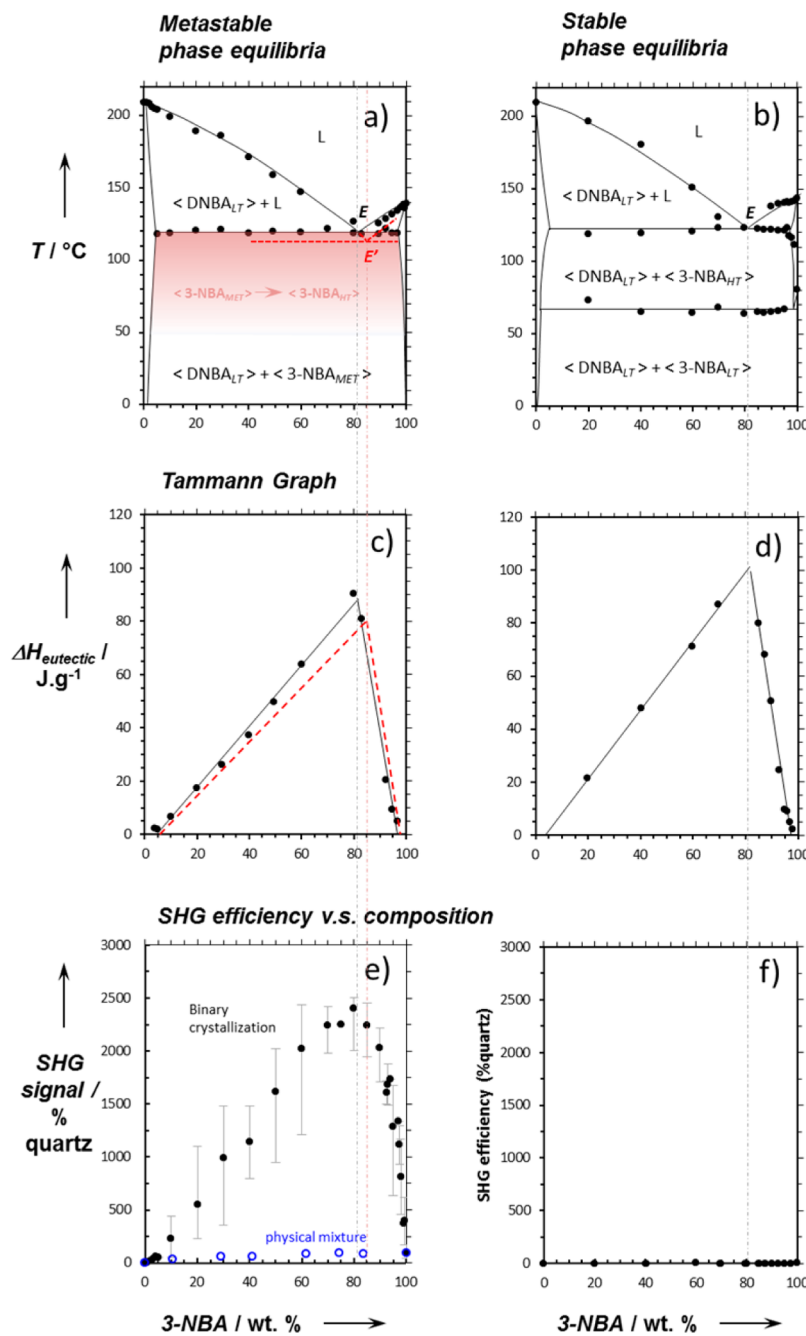


**Figure 9.** (Left) Metastable DNBA/3-NBA system; (Right) Stable DNBA/3-NBA system. The notation  $\langle \rangle$  indicates the corresponding phase, which might be a solid solution close to this corresponding phase. (a, b) Temperature vs composition phase equilibria for the  $\text{DNBA}_{LT}/\text{3-NBA}_{MET}$  and  $\text{DNBA}_{LT}/\text{3-NBA}_{LT}$  systems, respectively. Liquidus lines were constructed with the maximal deflection of the fusion peak, and eutectic invariants were constructed by considering the onset eutectic endotherms (see the Supporting Information for DSC results). The different solid phases prepared at room temperature were verified for each composition (see the Supporting Information for XRPD results). Solid lines correspond to stable equilibria; red dashed lines correspond to a possible location of the metastable equilibria. The widths of partial solid solution were determined with the Tammann graph (c, d), and solidus lines at other temperatures were drawn arbitrarily; (c, d) enthalpy vs composition plots (Tammann graph: calorimetry of the eutectic invariant) for the two systems (red dashed lines correspond to the possible Tammann graph for the metastable eutectic equilibrium); (e) SHG signal vs composition for the  $\text{DNBA}_{LT}/\text{3-NBA}_{MET}$  system. SHG intensities were normalized by considering  $\alpha$ -quartz (44  $\mu\text{m}$  average size) as a reference unit for the SHG signal. Error bars were computed over a sum of 5 different series of samples. The black filled circles and the blue open circles are associated, respectively, to the samples prepared by binary crystallization (DNBA and 3-NBA mixed together and crystallized from acetone by solvent evaporation) and to the samples prepared by physical mixture (DNBA and 3-NBA were crystallized separately from acetone before being mixed at several ratios); and (f) SHG signal vs composition for the stable  $\text{DNBA}_{LT}/\text{3-NBA}_{LT}$  system.

reported earlier, then they are not suspected to be present in the commercial product according to the DNBA synthesis.<sup>61,62</sup> This is not the case for 3-NBA, which is an intermediate material for DNBA production. Indeed, the most widespread

process in industry for DNBA synthesis is the reaction of benzoic acid with  $\text{BF}_3\text{N}_2\text{O}_5$  complex.<sup>61,62</sup> This reaction gives a mixture of DNBA (70% yield) and 3-NBA (9.3% yield),<sup>61</sup> and the two compounds must be separated and purified before use.

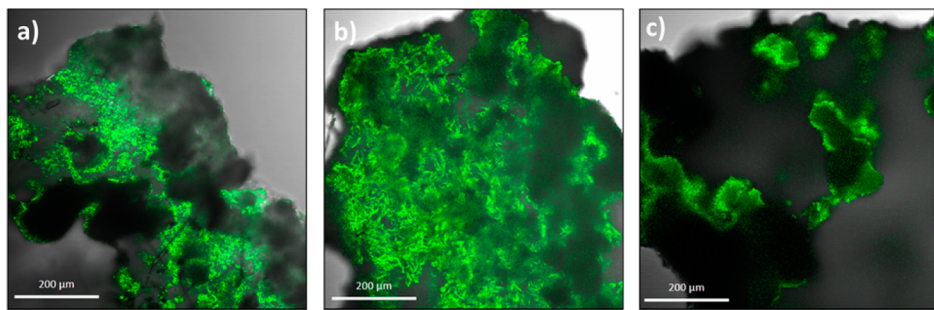


**Figure 10.** SHGM images of a polycrystalline sample (agglomerated) crystallized from acetone by solvent evaporation at different compositions: (a) hypoeutectic composition (40 wt % 3-NBA), (b) near-eutectic composition (80 wt % 3-NBA), and (c) hypereutectic composition (97 wt % 3-NBA). Green zones correspond to SHG-active domains, whereas dark zones correspond to either centrosymmetric domains or noncentrosymmetric domains under phase-mismatch conditions.

Ionic chromatography experiments performed on *Com*DNBA powder led to the detection of ca. 0.5 wt % 3-NBA in the samples. *Com*DNBA was then purified using semipreparative chromatography. The SHG analyses of the purified samples did not lead to any significant signal, confirming the relation between the SHG activity of *Com*DNBA and the presence of 3-NBA under its metastable polymorphic form (3-NBA<sub>MET</sub>).

In order to establish the relationship between the composition of both phases (DNBA and 3-NBA) and the intensity of the SHG signal, the metastable phase diagram between DNBA and 3-NBA was drawn. For comparison, the stable phase diagram was also studied.

**Heterogeneous Equilibria between DNBA and 3-NBA and SHG Studies.** For the construction of the metastable phase diagram between DNBA and 3-NBA (Figure 9a), samples were prepared by mixing DNBA and 3-NBA (both solids at room temperature) at several ratios and then crystallizing them by solvent evaporation from acetone at room temperature (see the Material and Methods). For the construction of the stable phase diagram (Figure 9b), samples were prepared by mixing *Com*DNBA and *Com*3-NBA at several ratios and then milling them without solvent. Crystallized powder samples were analyzed by XRPD and DSC (see the Supporting Information), which allowed us to construct the phase diagrams (Figure 9a,b). At room temperature, the solid phases are composed of DNBA<sub>LT</sub> and 3-NBA<sub>MET</sub> for the study of the metastable phase diagram and DNBA<sub>LT</sub> and 3-NBA<sub>LT</sub> for the study of the stable phase diagram. DSC results indicate that both phase diagrams show eutectic phase behavior. At ca. 70 °C, the polymorphic transition 3-NBA<sub>LT</sub> → 3-NBA<sub>HT</sub> is observed. The temperature of the polymorphic transition is lower compared to that of the pure 3-NBA compound, indicating that a eutectoid equilibrium ( $\langle\text{DNBA}_{\text{LT}}\rangle + \langle\text{3-NBA}_{\text{LT}}\rangle \leftrightarrow \text{liquid}$ ) probably exists.<sup>63</sup> For the metastable phase diagram, no irreversible polymorphic transition (3-NBA<sub>MET</sub> → 3-NBA<sub>HT</sub>) was found in the whole range of composition, but, as previously described for pure 3-NBA, the polymorphic transition could not be detected by DSC. Consequently, TR-SHG experiments were carried out on powder samples for each composition (see the Supporting Information) and confirm a progressive transition from 3-NBA<sub>MET</sub> toward 3-NBA<sub>HT</sub> upon heating. The evolution of the SHG signals vs the mass fraction in 3-NBA<sub>MET</sub> will be discussed later. This monotropic phase transition is schematized by the gradient colored red zone (Figure 9a). The metastable eutectic point ( $E'$ ) corresponding to the reaction ( $\langle\text{DNBA}_{\text{LT}}\rangle + \langle\text{3-NBA}_{\text{MET}}\rangle \leftrightarrow \text{liquid}$ ) had been located arbitrarily. This

metastable equilibrium might be very close to the stable one, as confirmed by TR-SHG experiments where 3-NBA<sub>MET</sub> was still present in a non-negligible proportion at high temperature. However, this transition is governed by kinetics, as confirmed by its monotropic character, and thus it was not possible to predict the precise location of  $E'$ . The enthalpy of the eutectic invariant was calculated for each sample in order to draw the Tammann graph corresponding to each phase diagram (Figure 9c,d). It was used to determine the precise eutectic composition and the range (in composition) of the solid–solid demixion at the eutectic temperature and therefore the ranges of solid solutions at the same temperature. From these data, one can see that similar results are found for both phase diagrams, indicating that the eutectic equilibrium corresponded to the ( $\langle\text{DNBA}_{\text{LT}}\rangle + \langle\text{3-NBA}_{\text{HT}}\rangle \leftrightarrow \text{liquid}$ ) reaction. The SHG efficiencies at room temperature for powder samples were measured (Figure 9e,f). As expected, the SHG signal remains null when 3-NBA<sub>LT</sub> is involved because it is a centrosymmetric phase. Of particular interest is the evolution of the SHG signal vs the mass fraction of 3-NBA when the metastable polymorph is involved. Indeed, the SHG signal was not found to evolve linearly with the proportion of 3-NBA<sub>MET</sub>. The maximal value of the SHG signal was found to be 20 times higher than the SHG signal of the pure noncentrosymmetric 3-NBA<sub>MET</sub> phase. It should be noted that even for the compositions with low 3-NBA content (e.g., 10 wt %) the SHG signals still exceed those of pure 3-NBA<sub>MET</sub>. The highest SHG signals were found close to the eutectic compositions, and variation of the SHG signal vs composition (Figure 9e) was found to be close to that of the Tammann graph (Figure 9c). To avoid confusion, note that the Tammann graph is associated with stable equilibrium ( $\langle\text{NBA}_{\text{LT}}\rangle + \langle\text{3-NBA}_{\text{HT}}\rangle \leftrightarrow \text{liquid}$ ) but that the Tammann graph associated with a metastable equilibrium ( $\langle\text{DNBA}_{\text{LT}}\rangle + \langle\text{3-NBA}_{\text{MET}}\rangle \leftrightarrow \text{liquid}$ ) might be close.

In the early 90s, several works<sup>64–68</sup> reported unusual values found for binary mixtures of *para*-nitroaniline and its derivatives but concluded that SHG signal enhancements were due to polymorphism,<sup>64–66</sup> co-crystal formation,<sup>67</sup> or impurity(ies).<sup>68</sup> In the present case, the unusual SHG behavior could originate from the formation of a suitable self-organized microstructure during solidification at the metastable eutectic point.

**The Eutectic Microstructure and SHG Signal Enhancement by Quasi-Phase-Matching (QPM) Process.** Considering eutectic binary systems, particular microstructures, such as lamellar or rod-like grains, constituted of the two phases are known to arise from eutectic solidification.<sup>69–71</sup> For organic

materials, the microstructures also arise, but they are often far from being regular.<sup>72–75</sup>

Indeed, eutectic microstructures are, among other parameters (such as the cooling rate), strongly dependent on the melting entropy of both phases. According to Jackson and Hunt's theory,<sup>71,76</sup> the crystallization behavior of any crystalline phase can be associated with an either faceted or nonfaceted growth, leading to a regular or more or less irregular microstructure, respectively. To predict such a behavior, it is common to use the so-called roughness parameter (or dimensionless melting entropy),  $\alpha = \Delta S_m/R$ , where  $\Delta S_m$  is the melting entropy of a given compound and  $R$  is the universal gas constant ( $R = 8.314 \text{ J mol}^{-1} \text{ K}^{-1}$ ). Above the threshold value of  $\alpha = 2$ , the crystallization front is smooth and the compound grows as faceted crystals. Consequently, the resulting microstructure is not regular. For most organic materials, the molecules are free to rotate in the liquid state, but they have a specific orientation in the crystal. Melting entropies for many of these materials are relatively high, e.g.,  $\alpha$  values around 6,<sup>72,77,78</sup> except in rare cases.<sup>79</sup> Unfortunately, the  $\alpha$  values for  $\langle\text{DNBA}_{\text{LT}}\rangle$  and  $\langle\text{3-NBA}_{\text{MET}}\rangle$  cannot be determined due to their conversion toward their high-temperature polymorphs. However, the  $\alpha$  values for  $\langle\text{DNBA}_{\text{HT}}\rangle$  and  $\langle\text{3-NBA}_{\text{HT}}\rangle$  are, respectively, 7.81 and 4.97, and thus enter in the common aforementioned range of values for most organic compounds.

The hypothesis of a formation of a microstructure was confirmed by our observation of samples of hypoeutectic, near-eutectic, and hypereutectic composition via SHGM. Indeed, in Figure 10a–c, a fine microstructure is clearly visible in grains issued from the powder. Obviously this microstructure is quite irregular, as predicted, but  $\langle\text{3-NBA}_{\text{MET}}\rangle$  domains are found to be relatively well-dispersed inside the centrosymmetric matrix ( $\langle\text{DNBA}_{\text{LT}}\rangle$ ) and to feature a certain kind of periodicity between the two phases. The crystal size distribution for the  $\langle\text{3-NBA}_{\text{MET}}\rangle$  domains inside the matrix varied from a few microns to a few tens of microns. No studies have been devoted to the determination of the precise average coherence length  $\langle l_c \rangle_{\langle\text{3-NBA}_{\text{MET}}\rangle}$ , but it was shown with previous results that SHG signals were greater for samples with a small crystal size distribution (Figure 5). Knowledge of the average coherence length requires (i) a large number of sieving fractions, which is experimentally very difficult to obtain, and (ii) a method to produce particles with a very small size distribution, such as micronization, but this is not possible in our case due to the sensitivity of  $\langle\text{3-NBA}_{\text{MET}}\rangle$  to mechanical stress. Another method to determine the coherence length is the Maker fringes method,<sup>80–82</sup> but it was also not possible to use this technique in our case because, before long, no single crystals could be isolated.

SHGM images evidence the existence of a fine periodical microstructure involving  $\langle\text{3-NBA}_{\text{MET}}\rangle$  (a non-phase-matchable (NPM) noncentrosymmetric phase). This could lead to a quasi-phase-matching (QPM) mechanism (i.e., with  $\langle\text{3-NBA}_{\text{MET}}\rangle$  domains below the average coherence length for  $\langle\text{3-NBA}_{\text{MET}}\rangle$ ), which would then produce a strong in the SHG signal. In the field of materials for SHG, quasi phase matching (QPM)<sup>30,83</sup> has been proposed to be an efficient technique to prevent destructive interference from occurring inside NPM crystals by the construction of optimized periodically patterned materials.<sup>12,84,85</sup> A QPM mechanism can also be observed in polycrystalline samples (random QPM)<sup>86–88</sup> or in multi-component samples as soon as the bulk is disrupted by defects,

leading to a certain periodicity in the material. In these last two cases, QPM is, of course, less efficient because it is less optimized. In our case, a QPM process probably occurs within the grains that feature the eutectic microstructure.

To support this hypothesis, physical mixtures between  $\langle\text{DNBA}_{\text{LT}}\rangle$  and  $\langle\text{3-NBA}_{\text{MET}}\rangle$  were prepared from pure samples of DNBA and 3-NBA crystallized from acetone (Figure 9e). In this case, the SHG signal was observed to evolve, as expected, linearly with the mass fraction of the noncentrosymmetric  $\langle\text{3-NBA}_{\text{MET}}\rangle$ . Indeed, for SHG measurements on powders, the dependence of the SHG signal with the number of noncentrosymmetric particles having an equivalent size distribution has been reported to be linear.<sup>18,23,88–90</sup> Hereafter, we propose a rational description of the results found (Figure 11) for binary eutectic mixtures.

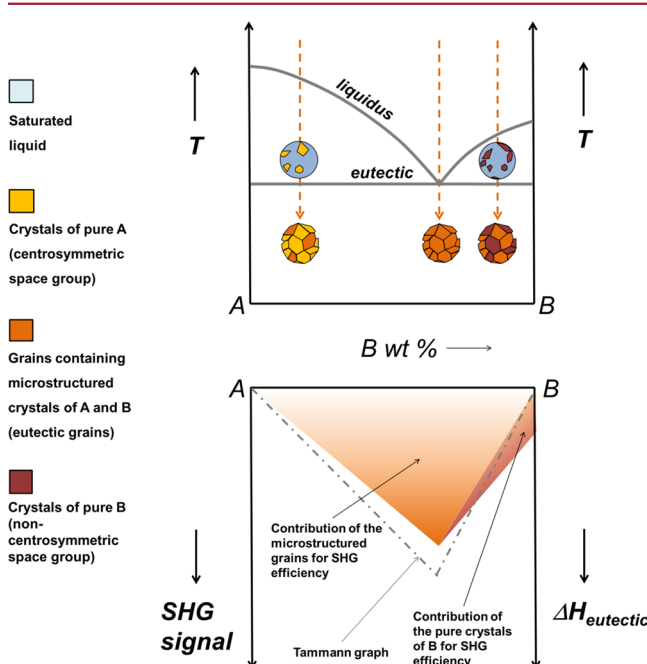


**Figure 11.** Schematic rationalization for the SHG signals found for powder samples in a eutectic phase diagram. (A) grains (yellow) correspond to a material crystallizing in a centrosymmetric space group (i.e., SHG cannot occur), and (B) grains (red) correspond to a material crystallizing in a noncentrosymmetric space group (not phase-matchable for SHG). Orange grains correspond to the eutectic microstructure (consisting in the alternation of  $\langle\text{DNBA}_{\text{LT}}\rangle$  and  $\langle\text{3-NBA}_{\text{MET}}\rangle$  small crystalline domains).

**Influence of the Proportion of Microstructured Grains on the SHG Signal.** Assuming that crystal size distribution and morphology are equivalent for each composition, or more precisely that each type of grain (i.e.,  $\langle\text{DNBA}_{\text{LT}}\rangle$ ,  $\langle\text{3-NBA}_{\text{MET}}\rangle$ , or eutectic) has the same crystal size distribution and similar morphologies, the overall SHG signal is the sum of the contributions to the SHG of each type of grain. For hypoeutectic compositions (ranging from 0 wt % 3-NBA toward the metastable eutectic composition  $E'$ ), solid phases are composed of pure crystallites of  $\langle\text{DNBA}_{\text{LT}}\rangle$  and the microstructured grains of eutectic composition. By application of the lever rule in the binary phase diagram, the proportion of microstructured grains evolves linearly toward the metastable eutectic composition  $E'$  (where the eutectic grains represent the total fraction of the sample). For hypoeutectic composi-

tions, the SHG signal was indeed experimentally found to evolve almost linearly with the proportion of microstructured grains. For hypereutectic compositions (ranging from the metastable eutectic composition  $E'$  toward the pure 3-NBA<sub>MET</sub>), the decrease in the SHG signal with composition could be understood by a decrease of the fraction of eutectic grains. Of course, contrary to that for a hypoeutectic composition, the pure 3-NBA<sub>MET</sub> crystallites bring an extra, but small, contribution to the overall SHG signal. This statement, i.e., the application of the lever rule to correlate the SHG signal with the proportion of each type of grain, is, of course, oversimplified. Indeed, eutectic solidification is strongly governed by kinetic parameters, and a full understanding of the microstructure should take into account many parameters that are presented in the next section.

**Thermodynamic and Kinetic Considerations on the Eutectic Microstructure Features of Organic Molecular Compounds.** This section is dedicated to the possible deviation from ideality when considering eutectic solidification. Indeed, the analyzed solid mixtures were obtained from rapid solvent evaporation (i.e., where growth kinetics play an important role in the resulting solid composition). If the quantity of microstructured grains (Figure 10) fits, apparently, well with the composition (i.e., the closer to the eutectic composition, the higher the proportion of the eutectic microstructure), then verification of the applicability of the lever rule for determining the true fraction of  $\langle \text{DNBA}_{\text{LT}} \rangle$  grains, grains at the eutectic composition ( $E'$ ), and  $\langle 3\text{-NBA}_{\text{MET}} \rangle$  grains would require a very large number of 3D images and adequate algorithms for zone distinction and particle counting. Moreover, the growth rate of  $\langle \text{DNBA}_{\text{LT}} \rangle$ ,  $\langle 3\text{-NBA}_{\text{MET}} \rangle$ , and the solid at the eutectic composition must be understood in order to verify the true application of the lever rule in the determination of the corresponding mass ratios of each of them when rapid crystallization methods are involved. For example, in some cases, the crystallization of a liquid mixture at the eutectic composition does not necessarily lead to a resulting solid composed of 100% of the typical eutectic microstructured grains. In other cases, the resulting solid exhibits only a fine microstructure, whereas the initial liquid mixture is not at the eutectic composition.<sup>71,76,91–95</sup> These precipitation anomalies have been referenced in the literature as quasi-eutectics<sup>93</sup> or irregular eutectics<sup>96</sup> and have been generalized through the concept of coupled growth.<sup>71</sup> There is actually a limited range of compositions where the two crystalline phases can grow in a coupled manner at the eutectic composition.<sup>76</sup> However, the qualitative estimation of this coupled growth zone requires the knowledge of the melting entropies of each compound or extensive and accurate microscopic experiments. This was not possible in our case with classical optical microscopy because both DNBA and 3-NBA have a similar appearance in the solid state. These precipitation anomalies, for example, could explain the flattening of the SHG signal observed for near-eutectic compositions.

Besides these possible deviations from ideality in eutectic systems, we cannot exclude for the DNBA/3-NBA system that a certain amount of amorphous material is produced through the crystallization process, as the XRPD patterns show broad diffraction peaks (see Supporting Information).

Furthermore, the crystallized binary mixtures were obtained from acetone; therefore, it is necessary to consider the ternary phase diagram, DNBA/3-NBA/acetone. As the solvent was totally evaporated in each sample, we considered our results

based only on the binary phase diagram DNBA<sub>LT</sub>/3-NBA<sub>MET</sub>. Nevertheless, a possible deviation of the invariant composition from the binary system DNBA<sub>LT</sub>/3-NBA<sub>MET</sub> to the ternary system DNBA<sub>LT</sub>/3-NBA<sub>MET</sub>/acetone at room temperature (temperature of crystallization), leading to possible segregation, could be possible, i.e., a mixture crystallized from a solvent at the eutectic composition does not necessarily lead to 100% microstructured grains. Nevertheless, the identification of the invariant point for the metastable ternary phase diagram would be rather difficult, as the process of crystallization was fast (a long slurry of 3-NBA<sub>MET</sub> in usual solvents led to the conversion toward 3-NBA<sub>LT</sub>). This is why the aforementioned discussion considered only the metastable binary phase diagram instead of the metastable ternary system.

The drawback of the crystallization-evaporation method is that it produces relatively small agglomerated grains (typically between 50 and 300  $\mu\text{m}$  in our experiments) associated with a broad particle size distribution. The result is that inside a polycrystalline grain the repetition order of each crystalline phase is relatively poor and, as previously mentioned, has random orientation. Obviously the microstructure features could be favored if melt crystallizations were used, e.g., leading to more regular microstructures (such as layered solid films), but this is restricted to thermally stable materials. DNBA and 3-NBA underwent sublimation at high temperature (above ca. 100 °C), which limited, in our case, the crystallization mode to the solvent-evaporation method. Crystallization from the melt in closed vials by rapid quenching in an ice bath was also performed, but a non-negligible proportion of 3-NBA<sub>HT</sub> polymorph was found in the crystallized samples. The SHG signals remain higher in the near-eutectic range, but the results showed a great variability over the different experiments (see Supporting Information). SHG signals were found to be lower than those found for powders crystallized by the solvent-evaporation method. Because the undercooling temperature was high (from ca. 200 to 0 °C in the present case), the coupled growth zone might also be large.

**Detection of 3-NBA<sub>MET</sub> Impurity at Low Levels Inside a DNBA Matrix.** The unusual enhancement in the SHG signal by the QPM mechanism inside the microstructured grains explained why a few tenths of a weight % of 3-NBA could be detected. For powder SHG measurements, it is commonly accepted that a signal of 0.1%<sup>29</sup> (or even lower)<sup>25</sup> of the  $\alpha$ -quartz reference signal could be considered a SHG signal sufficient to distinguish a noncentrosymmetric phase. For powder samples crystallized from the eutectic composition, the SHG signal was found to be in the range of 2000% of the reference  $\alpha$ -quartz signal, i.e., the detection limit for 3-NBA<sub>MET</sub> content inside the DNBA<sub>LT</sub> matrix could be considered as being below 50 ppm by weight.

SHGM analyses were performed on ComDNBA as well as on DNBA large crystals (Figure 12). The results show that the zones of noncentrosymmetry (in green) were localized randomly as clusters in the material, which may correspond to the (small) content of eutectic microstructured grain.

Both powder SHG and SHGM studies highlight the high threshold level of impurity detection, which is in accordance with other previous works.<sup>25,97</sup> Thus, the use of such techniques to complement classical characterization techniques (e.g., chromatography, spectroscopy, XRPD, DSC) appears to be relevant, e.g., in the pharmaceutical sciences, where purity is a pivotal issue.

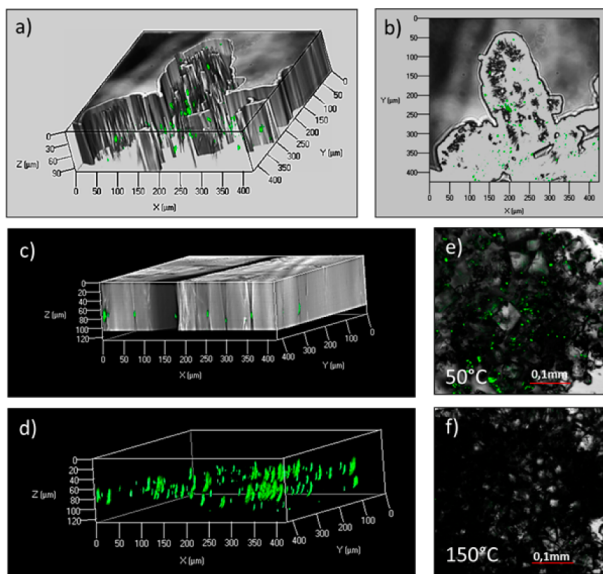


**Figure 12.** Combined SHG and optical microscopy images for ComDNBA powder and large crystal. SHG active areas appear in green: (a) in volume and (b) in surface. The dimensions of the noncentrosymmetric zones are a few micrometers to a few tens of micrometers. (c) Combined SHG and optical microscopy image for the surface of single crystals (the black line at the center of the image corresponds to a twin plan between two single crystals); (d) the same image with only the SHG active zones; (e) ComDNBA powder sample after annealing at 50 °C for 4 h; and (f) ComDNBA powder sample after annealing at 120 °C for 4 h showing that the SHG signal vanishes because of 3-NBA monotropic conversion.

Because a partial solid solution could exist at low 3-NBA content (i.e., ca. 5 wt % of 3-NBA content inside DNBA at the eutectic temperature), it was also envisaged that a solid solution could be formed at ambient temperature (probably containing few ppm of 3-NBA content). In this case, another mechanism to explain the SHG activity could be proposed: the formation of mixed crystals<sup>58,98</sup> wherein the matrix crystals (herein, DNBA) include impurities (herein, 3-NBA) in a nonuniform fashion during their growth, such as growth-induced polarity formation,<sup>58</sup> leading to a lowering of the global symmetry of the crystals.<sup>99</sup> Such symmetry lowering can lead to an SHG signal as soon as the inversion center is removed (e.g., from point group 2/m toward subgroups m, 2, or 1). These symmetry lowering effects have been found in many examples of solid solutions among organic materials.<sup>100–102</sup> Through this symmetry lowering process, centrosymmetric materials have also been proposed earlier as a matrix for polar alignment of guest molecules with the aim of fashioning a new type of material for SHG.<sup>103</sup> It was also reported that such mixed crystals could be observed through SHGM,<sup>104,105</sup> but it is necessary to have crystals thicker than the coherence length for this type of study (i.e., plate-like crystals of a few hundred nanometers toward a few micrometers in height), which, in our case, could not be isolated for SHGM observations. This growth-induced property of symmetry lowering has not previously been investigated in our case because in almost the entire range of the DNBA/3-NBA phase diagram the powder samples corresponded to a demixion of both phases in the solid state and thus the major contribution to the SHG signal arises from (i) the fraction in the noncentrosymmetric phase (3-NBA<sub>MET</sub>) and (ii) its organization inside the matrix (which defines the microstructure). We also note that such

growth-induced polarity formation can be observed in a single molecule compound (i.e., self-poisoning),<sup>99,106</sup> including nitro-derivative compounds.<sup>107</sup> However, we do not believe that such disorder could generate a sufficient SHG signal to be detectable by our apparatus, as all reported centrosymmetric powders used in the laboratory (which could exhibit the same defect) did not generate any detectable SHG signal (data not shown), contrary to that for the ComDNBA and RecDNBA powder samples.

A long annealing of RecDNBA above 120 °C caused the SHG signal to vanish, but when it was submitted to crystallization by solvent evaporation the SHG signal reappeared. This is in accordance with the thermal behavior of 3-NBA<sub>MET</sub>, which can undergo a polymorphic transition at elevated temperature. From a general point of view, 3-NBA<sub>MET</sub> was found to be more stable inside the DNBA<sub>LT</sub> matrix than the pure sample, and the SHG signal could be observed in the commercial product even after several years of storage at room temperature. This may be due to a poorly cooperative solid–solid transition process (domain dispersion inside a matrix). This observation was supported by isothermal transformations of pure 3-NBA<sub>MET</sub> and 3-NBA<sub>MET</sub> inside ComDNBA. Both were studied by monitoring the time dependence of the SHG signal at 85 °C. The results clearly show that no conversion occurs for 3-NBA<sub>MET</sub> inside the DNBA matrix after 6 days (Figure 13a), whereas the total conversion from 3-NBA<sub>MET</sub> toward 3-NBA<sub>HT</sub> occurred in few days at 85 °C (Figure 13b).

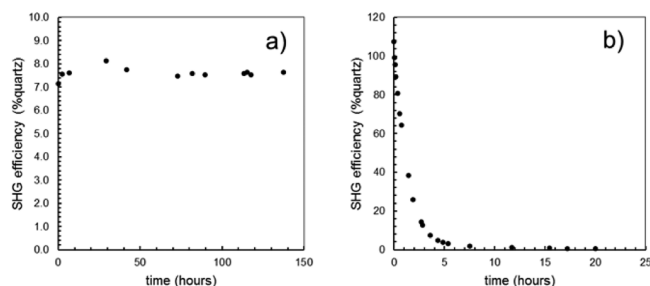


**Figure 13.** Isothermal SHG measurements on ComDNBA (a) and 3-NBA<sub>MET</sub> (b) at 85 °C.

A template effect of DNBA to prevent the conversion could also be envisaged, but this has not been demonstrated yet. Further investigations concerning the interactions between 3-NBA<sub>MET</sub> and 3,5-DNBA are required to improve the understanding of this host–guest association on mesoscale.

**Occurrence and Future Directions.** Our observation of SHG signal enhancement in a eutectic microstructure should *a priori* concern only systems including a noncentrosymmetric phase, which is NPM for SHG (we exclude here very fine (nanometric) microstructure, where other effects may appear). This is, therefore, restricted to a limited number of possible candidates among noncentrosymmetric phases. Nevertheless, it should be noted that eutectic phase behavior is widely encountered for organic compounds.<sup>108,109</sup> NPM materials could then be mixed with an almost infinite number of other components (or compounds) to generate a huge number of possible adequate eutectic microstructures (e.g., in terms of geometrical motifs, their size, their orientation, etc.). This may reside in the choice of suitable binary mixtures as well as in the use of suitable crystallization conditions. Indeed, the advantage in forming eutectic materials instead of using the pure components is that many properties could arise from the

particular arrangements of both constituents' crystalline phases, such as the QPM process when the noncentrosymmetric NPM crystalline domains included in the eutectic grains are close to the coherence length, below the coherence length, or close to an odd multiple of the coherence length. In contrast, a eutectic microstructure displaying domains with an average size of twice (or an even number) the coherence length should not be suitable for producing SHG signal enhancement. In this nonoptimized case, the SHG signal should be very weak.

To extend the description of the aforementioned results, i.e., the apparent rationale for selecting the optimum composition for the maximal SHG signal, 3-NBA was mixed with benzoic acid (BA) (see the Supporting Information). The process of crystallization was similar, and a similar tendency for an increase in the SHG signal was found. However, the powder sample at the eutectic composition showed an increase of only four times compared to that for pure 3-NBA<sub>MET</sub> (compared to ca. 20 times in the case of the DNBA/3-NBA system). This is due to the key role played by the centrosymmetric matrix, as different matrices could lead to different crystallization conditions and, therefore, to different microstructures. Indeed, the SHG signal for microstructured grains strongly depends on the dimensions of the non-phase-matchable domains (i.e., an optimal SHG signal is obtained if their average size is below or close to the coherence length) and the manner in which they are homogeneously dispersed inside the grain. Admittedly, SHG signal enhancement in eutectic binary mixtures might not be a systematic outcome since the SHG signal strongly depends on (i) the pure components selected and (ii) the sample preparation, i.e., if a suitable microstructure can be formed.

On the basis of the preliminary results described with the DNBA/3-NBA system, a conglomerate of atropoisomers was recently studied by SHG and showed SHG signal enhancement at the eutectic composition.<sup>110</sup> (A conglomerate corresponds to a mixture of mirror-image crystallized phases exhibiting symmetrical enantiomeric excesses.<sup>95</sup> The eutectic or eutectoid point is located at the racemic composition (50:50 in both enantiomers).) The eutectic microstructure was found to be of multiepitaxial-type, which led to a favorable periodicity for SHG enhancement. If the multiepitaxial-type microstructure is well-adapted, then such materials could be adequate candidates for QPM devices. This has already been demonstrated in Langmuir–Blodgett films of chiral materials.<sup>111,112</sup> Phase diagrams between enantiomers,<sup>8</sup> including those with multiepitaxial-type microstructures,<sup>110,113</sup> complex polymorphism,<sup>43,114,115</sup> and solvated systems (which can lead to porous microstructures during desolvation),<sup>116</sup> have been extensively studied due to their importance in the pharmaceutical industry and therefore they provide many potential binary systems for SHG applications.

However, in general, the observation of such SHG signal enhancement in other eutectic systems of organic compounds (including enantiomers) has, for the moment, been shown to be inconclusively correlated with the eutectic composition (data not shown), even if higher SHG signals have often been observed for intermediate compositions. (This study has been restricted to binary organic mixtures containing (i) a centrosymmetric phase and a noncentrosymmetric phase (which is NPM for SHG) and (ii) two noncentrosymmetric phases (NPM) (including binary systems of enantiomers). Many of these systems were obtained by the solvent-evaporation method.) This indicates the difficulties in obtaining suitable microstructures to produce a sufficient enhancement in

the SHG signal by the QPM process. Indeed, for noncentrosymmetric NPM materials, coherence lengths are often situated in the range 1–20 μm,<sup>83,117</sup> which requires a solidification method to induce the formation of a microstructure with finer domains. This is, of course, jeopardized when considering the eutectic solidification of organic compounds. The organic crystalline phases often exhibit faceted growth due to their relatively high melting entropy, leading to a larger and less regular eutectic microstructure than that observed in metallic<sup>69–71</sup> and oxide systems.<sup>118–121</sup>

In the field of nonlinear optical materials, oxide and inorganic materials represent a rich source of noncentrosymmetry,<sup>11,122–127</sup> where several of them have been reported to be NPM for SHG.<sup>127–131</sup> Also, phase diagrams have been studied in some cases, e.g., to find new defined compounds that are PM for SHG in a ternary system<sup>131</sup> or to find the optimal composition in a binary solid solution.<sup>129,132,133</sup> Thus, the study of eutectic systems may be of great relevance to overcome the problem of phase matchability for SHG when NPM oxides are involved. Furthermore, it is well-known that techniques to produce bulk and regular microstructured eutectic materials have been developed, such as the micro pulling-down method.<sup>121,134–136</sup>

#### Parallels with Other Materials Science Applications.

This present study also examines the more general concept of the arrangement of the matter vs the observed physical properties. For efficient optoelectronic devices (for photovoltaic applications), the use of binary eutectic mixtures has already been reported.<sup>137–139</sup> Müller et al.<sup>138</sup> showed that in organic binary mixtures featuring a eutectic phase behavior the optimal device performance (in terms of short-circuit current density) was situated in the near-eutectic range because of enhanced donor–acceptor interface area. Their results on the observed performance vs composition strongly match with our reported observations.

The 21st century has also been marked by the rapid emergence of metamaterials<sup>140–142</sup> and photonic crystals.<sup>12,143–145</sup> They both have an artificial periodical structure and have been proposed for use in many applications including SHG.<sup>12,141–145</sup> Recently, Pawlak et al.<sup>121,146</sup> showed the potential of eutectic forming systems as an alternative to metamaterials and photonic crystals. Self-organized eutectic solidification, by its nature, can result in a very interesting spatial distribution of several materials with adequate geometrical motifs, which may afford enhanced electromagnetic properties.

#### CONCLUSIONS

This study shows that the weak SHG signal observed on the commercial powder of DNBA is associated with the presence of a small amount of impurity (<0.5 wt %), 3-NBA, which crystallized as a metastable SHG-active phase. The presence of this impurity was quantified by ionic chromatography experiments, and SHGM showed that these impurities appear as clusters in the bulk material. The phase equilibria between DNBA and 3-NBA has revealed a simple eutectic behavior in which 3-NBA<sub>MET</sub> is obtained as a crystalline phase by fast solvent evaporation in standard organic solvents. SHGM studies have highlighted the formation of a fine self-assembled eutectic microstructure that is suitable for a QPM process and that consequently induces SHG signal enhancements in compositions of the near-eutectic range compared to that for the pure noncentrosymmetric phase. This study gives a possible

new route for QPM using a eutectic microstructure as soon as it is tunable. Indeed, almost every entity can be used as the matrix (in complement with the noncentrosymmetric NPM phase), and the crystallization methods can be adapted to design the most appropriate geometrical features of this microstructure.

This study also features an interesting bridge between nonlinear optical properties (SHG in this study) and heterogeneous equilibria (with at least one constituent is a noncentrosymmetric phase). It highlights the potential of SHG-based techniques (powder SHG, TR-SHG, and SHGM) to study multiphase samples and their microstructures and, therefore, enlarges their fields of application in materials science. Furthermore, from a materials point of view, this study offers many perspectives to find optimal compositions supporting eutectic multiphase samples for nonlinear optical applications as well as the for the detection and characterization of possible new intermediate compounds suitable for frequency-conversion applications.

## ■ ASSOCIATED CONTENT

### Supporting Information

X-ray crystallographic data for  $\text{DNBA}_{\text{LT}}$ , XRPD vs temperature for  $\text{DNBA}_{\text{LT}}$ , 3-NBA<sub>MET</sub>, and 3-NBA<sub>LT</sub>, XRPD, DSC, and TR-SHG for the  $\text{DNBA}_{\text{LT}}/3\text{-NBA}_{\text{MET}}$  system at various compositions. XRPD and DSC for the  $\text{DNBA}_{\text{LT}}/3\text{-NBA}_{\text{LT}}$  system at various compositions. XRPD and DSC for the BA/3-NBA<sub>MET</sub> system at various compositions. Phase diagram, Tammann graph, and SHG signal vs composition graph for the BA/3-NBA<sub>MET</sub> system. SHG vs composition graph for the  $\text{DNBA}_{\text{LT}}/3\text{-NBA}_{\text{MET}}$  system (melt crystallization). This material is available free of charge via the Internet at <http://pubs.acs.org>.

## ■ AUTHOR INFORMATION

### Corresponding Author

\*E-mail: valerie.dupray@univ-rouen.fr.

### Notes

The authors declare no competing financial interest.

## ■ ACKNOWLEDGMENTS

Dr. Christine Terryn, Plateforme Imagerie Cellulaire et Tissulaire IBISA de l'Université de Reims Champagne Ardenne, is greatly acknowledged for second harmonic generation microscopy analysis. Marie Vaccaro, SMS EA3233, Université de Rouen, is greatly acknowledged for ionic chromatography analysis.

## ■ REFERENCES

- (1) Coquerel, G. *Chem. Soc. Rev.* **2014**, *43*, 2286–2300.
- (2) Mullin, J. W. *Crystallization*, 4th ed.; Butterworth-Heinemann: Oxford, 2001.
- (3) Hulliger, J. *Angew. Chem., Int. Ed. Engl.* **1994**, *33*, 143–162.
- (4) Bernstein, J. *Cryst. Growth Des.* **2011**, *11*, 632–650.
- (5) Lee, E. H. *Asian J. Pharm. Sci.* **2014**, *9*, 163–175.
- (6) Coquerel, G. *Chem. Eng. Process.* **2006**, *45*, 857–862.
- (7) Schultheiss, N.; Newman, A. *Cryst. Growth Des.* **2009**, *9*, 2950–2967.
- (8) Coquerel, G. *Enantiomer* **2000**, *5*, 481–498.
- (9) Threlfall, T. L. *Analyst* **1995**, *120*, 2435–2460.
- (10) Aaltonen, J.; Allesø, M.; Mirza, S.; Koradia, V.; Gordon, K. C.; Rantanen, J. *Eur. J. Pharm. Biopharm.* **2009**, *71*, 23–37.
- (11) Kurtz, S. K. *IEEE J. Quantum Electron.* **1968**, *QE-4*, 578–584.
- (12) Arie, A.; Voloch, N. *Laser Photonics Rev.* **2010**, *4*, 355–373.
- (13) Kurtz, S. K.; Dougherty, J. P. In *Systematic Materials Analysis*; Richardson, J. H., Peterson, R. V., Eds.; Academic Press, Inc.: New York, 1978.
- (14) Sutherland, R. L.; McLean, D. G.; Kirkpatrick, S. *Handbook of Nonlinear Optics*, 2nd ed.; Marcel Dekker, Inc.: New York, 2003.
- (15) Bloembergen, N. *Nonlinear Optics*; 4th ed.; World Scientific: River Edge, NJ, 1996.
- (16) Franken, P. A.; Ward, J. F. *Rev. Mod. Phys.* **1968**, *35*, 23–39.
- (17) Ok, K. M.; Chi, E. O.; Halasyamani, P. S. *Chem. Soc. Rev.* **2006**, *35*, 710–717.
- (18) Allen, F. H. *Acta Crystallogr., Sect. B* **2002**, *58*, 380–388.
- (19) Kurtz, S. K.; Perry, T. T. *J. Appl. Phys.* **1968**, *39*, 3798–3813.
- (20) Coda, A.; Pandarese, F. *J. Appl. Crystallogr.* **1976**, *9*, 193–198.
- (21) Galland, A.; Dupray, V.; Berton, B.; Morin-Grognet, S.; Sanselme, M.; Atmani, H.; Coquerel, G. *Cryst. Growth Des.* **2009**, *9*, 2713–2718.
- (22) Aramburu, I.; Ortega, J.; Folcia, C. L.; Etxebarria, J.; Illarramendi, M. a.; Breczewski, T. *J. Appl. Phys.* **2011**, *109*, 113105.
- (23) Aramburu, I.; Ortega, J.; Folcia, C. L.; Etxebarria, J. *Appl. Phys. B: Lasers Opt.* **2013**, *1*–23.
- (24) Aramburu, I.; Ortega, J.; Folcia, C. L.; Etxebarria, J. *Appl. Phys. Lett.* **2014**, *104*, 071107.
- (25) Clevers, S.; Simon, F.; Dupray, V.; Coquerel, G. *J. Therm. Anal. Calorim.* **2013**, *112*, 271–277.
- (26) Clevers, S.; Simon, F.; Sanselme, M.; Dupray, V.; Coquerel, G. *Cryst. Growth Des.* **2013**, *13*, 3697–3704.
- (27) Thomas, S. P.; Nagarajan, K.; Guru Row, T. N. *Chem. Commun.* **2012**, *48*, 10559–10561.
- (28) Rawle, C. B.; Lee, C. J.; Strachan, C. J.; Payne, K.; Manson, P. J.; Rades, T. *J. Pharm. Sci.* **2006**, *95*, 761–768.
- (29) Dougherty, J. P.; Kurtz, S. K. *J. Appl. Crystallogr.* **1976**, *9*, 145–158.
- (30) Armstrong, J. A.; Bloembergen, N.; Ducuing, J.; Pershan, P. S. *Phys. Rev.* **1962**, *127*, 1918–1939.
- (31) Bayarjargal, L.; Winkler, B. Z. *Kristallogr.—Cryst. Mater.* **2014**, *229*, 92–100.
- (32) Henson, B.; Asay, B.; Sander, R.; Son, S.; Robinson, J.; Dickson, P. *Phys. Rev. Lett.* **1999**, *82*, 1213–1216.
- (33) Hall, R. C.; Paul, I. C.; Curtin, D. Y. *J. Am. Chem. Soc.* **1988**, *110*, 2848–2854.
- (34) Zhang, Y.; Ye, H.-Y.; Zhang, W.; Xiong, R.-G. *Inorg. Chem. Front.* **2014**, *1*, 118–123.
- (35) Clevers, S.; Rougeot, C.; Simon, F.; Dupray, V.; Coquerel, G. *J. Mol. Struct.* **2014**, *1078*, 61–67.
- (36) Freund, I.; Deutsch, M.; Sprecher, A. *Biophys. J.* **1986**, *50*, 693–712.
- (37) Gannaway, J. N.; Sheppard, C. J. R. *Opt. Quantum Electron.* **1978**, *10*, 435–439.
- (38) Kissick, D. J.; Wanapun, D.; Simpson, G. J. *Annu. Rev. Anal. Chem.* **2011**, *419*–437.
- (39) Toth, S. J.; Madden, J. T.; Taylor, L. S.; Marsac, P.; Simpson, G. J. *Anal. Chem.* **2012**, *84*, 5869–5875.
- (40) Xu, J.; Bao, J.; Guo, B.; Ma, H.; Yun, T.; Gao, L. *Polymer* **2007**, *48*, 348–355.
- (41) Beermann, J.; Bozhevolnyi, S. *Phys. Rev. B* **2004**, *69*, 155429.
- (42) Yokota, H.; Kaneshiro, J.; Uesu, Y. *Phys. Res. Int.* **2012**, *704634*.
- (43) Chowdhury, A. U.; Dettmar, C. M.; Sullivan, S. Z.; Zhang, S.; Jacobs, K. T.; Kissick, D. J.; Maltais, T.; Hedderich, H. G.; Bishop, P. A.; Simpson, G. J. *J. Am. Chem. Soc.* **2014**, *136*, 2404–2412.
- (44) DeWalt, E. L.; Sullivan, S. Z.; Schmitt, P. D.; Muir, R. D.; Simpson, G. J. *Anal. Chem.* **2014**, *86*, 8448–8456.
- (45) Van der Veen, M. A.; Vermoortele, F.; De Vos, D. E.; Verbiest, T. *Anal. Chem.* **2012**, *84*, 6378–6385.
- (46) Van der Veen, M. A.; Vermoortele, F.; De Vos, D. E.; Verbiest, T. *Anal. Chem.* **2012**, *84*, 6386–6390.
- (47) Prince, P.; Fronczek, F. R.; Gandour, R. D. *Acta Crystallogr., Sect. C: Cryst. Struct. Commun.* **1991**, *47*, 895–898.
- (48) Dhaneshwar, N. N.; Tavale, S. S.; Pant, L. M. *Acta Crystallogr.* **1974**, *B30*, 583–587.

- (49) Dhaneshwar, N. N.; Kulkarni, A. G.; Tavale, S. S.; Pant, L. M. *Acta Crystallogr.* **1978**, *B31*, 1978–1980.
- (50) Baur, W. H.; Kassner, D. *Acta Crystallogr., Sect. B: Struct. Sci.* **1992**, *48*, 356–369.
- (51) Behrnd, N.-R.; Labat, G.; Venugopalan, P.; Hulliger, J.; Bürgi, H.-B. *Cryst. Growth Des.* **2010**, *10*, 52–59.
- (52) Jones, A. O. F.; Blagden, N.; McIntyre, G. J.; Parkin, A.; Seaton, C. C.; Thomas, L. H.; Wilson, C. C. *Cryst. Growth Des.* **2013**, *13*, 497–509.
- (53) Collet, E.; Lemée-Cailleau, M. H.; Buron-Le Cointe, M.; Cailleau, H.; Wulff, M.; Luty, T.; Koshihara, S. Y.; Meyer, M.; Toupet, L.; Rabiller, P.; Techert, S. *Science* **2003**, *300*, 612.
- (54) Sunagawa, I. *Crystals: Growth, Morphology and Perfection*; Cambridge University Press: Cambridge, 2005.
- (55) Brooks, R.; Horton, A. T.; Torgesen, J. L. *J. Cryst. Growth* **1968**, *2*, 279–283.
- (56) Zhang, J.; Zhang, S.; Wang, Z.; Zhang, Z.; Wang, S.; Wang, S. *Angew. Chem., Int. Ed.* **2011**, *50*, 6044–6047.
- (57) Fontana, P.; Schefer, J.; Pettit, D. *J. Cryst. Growth* **2011**, *324*, 207–211.
- (58) Hulliger, J.; Wüst, T.; Brahimi, K.; Burgener, M.; Aboulfadl, H. *New J. Chem.* **2013**, *37*, 2229–2235.
- (59) Yang, G.; Weng Ng, S. *Cryst. Res. Technol.* **2007**, *42*, 201–206.
- (60) Etter, M. C.; Frankenbach, G. M. *Chem. Mater.* **1989**, *1*, 10–12.
- (61) Bachman, G. B.; Dever, J. L. *J. Am. Chem. Soc.* **1958**, *80*, 5871–5873.
- (62) Tang, Z.; Jin, J.; Yu, X.; Zhang, Z.; Liu, H. *Thermochim. Acta* **2011**, *517*, 105–114.
- (63) Coquerel, G. *Chem. Eng. Technol.* **2006**, *29*, 182–186.
- (64) Okamoto, N.; Abe, T.; Chen, D. Y.; Fujimura, H.; Matsushima, R. *Opt. Commun.* **1990**, *74*, 421–424.
- (65) Tasaka, S.; Abe, T.; Matsushima, R.; Suzuki, M.; Chen, D. Y.; Okamoto, N. *Jpn. J. Appl. Phys.* **1991**, *30*, 296–300.
- (66) Wakita, K.; Sonoda, N.; Shimizu, T.; Kaida, S. *J. Appl. Phys.* **1991**, *69*, 545–547.
- (67) Matsushima, R.; Takeshita, H.; Okamoto, N. *J. Mater. Chem.* **1991**, *1*, 591–593.
- (68) Matsushima, R.; Hiramatsu, K.; Okamoto, N. *J. Mater. Chem.* **1993**, *3*, 1045–1048.
- (69) Porter, D. A.; Easterling, K. E. *Phase Transformations in Metals and Alloys*, 2nd ed.; Chapman & Hall: London, 1992.
- (70) Callister, W. D. *Fundamentals of Materials Science and Engineering*, 5th ed.; John Wiley & Sons, Inc.: New York, 2001; pp 281–322.
- (71) Jackson, K. A. *Kinetic Processes: Crystal Growth, Diffusion, and Phase Transformations in Materials*; Wiley-VCH: Weinheim, 2004; pp 361–379.
- (72) Laudise, R. A.; Carruthers, J. R.; Jackson, K. A. *Annu. Rev. Mater. Sci.* **1971**, *1*, 253–288.
- (73) Sharma, B. L.; Sharma, N. K.; Bassi, P. S. *J. Cryst. Growth* **1984**, *67*, 633–638.
- (74) Podolinsky, V. V.; Taran, Y. N.; Drykin, V. G. *J. Cryst. Growth* **1986**, *74*, 57–66.
- (75) Rai, U. S.; Shekhar, H. *Cryst. Res. Technol.* **1994**, *29*, 533–542.
- (76) Hunt, J. D.; Jackson, K. A. *Trans. Met. Soc. AIME* **1966**, *236*, 843–852.
- (77) Yalkowsky, S. H. *Ind. Eng. Chem. Fundam.* **1979**, *18*, 108–111.
- (78) Yoon, T. J.; Youn, Y.-S.; Son, W.-S.; Seo, B.; Ahn, K. H.; Lee, Y.-W. *Cryst. Growth Des.* **2013**, *13*, 3481–3489.
- (79) Jackson, K. A.; Hunt, J. D. *Acta Metall.* **1965**, *13*, 1212–1215.
- (80) Maker, P. D.; Terhune, R. W.; Nisenoff, M.; Savage, C. M. *Phys. Rev. Lett.* **1962**, *8*, 21–23.
- (81) Jerphagnon, J.; Kurtz, S. K. *J. Appl. Phys.* **1970**, *41*, 1667–1681.
- (82) Herman, W. N.; Hayden, L. M. *J. Opt. Soc. Am. B* **1995**, *12*, 416–427.
- (83) Fejer, M. M.; Magel, G. A.; Jundt, D. H.; Byer, R. L. *IEEE J. Quantum Electron.* **1992**, *28*, 2631–2654.
- (84) Houé, M.; Townsend, P. D. *J. Phys. D: Appl. Phys.* **1995**, *28*, 1747–1763.
- (85) Fiore, A.; Berger, V.; Rosencher, E.; Bravetti, P.; Nagle, J. *Nature* **1998**, *391*, 463–466.
- (86) Baudrier-Raybaut, M.; Haïdar, R.; Kupecek, P.; Lemasson, P.; Rosencher, E. *Nature* **2004**, *432*, 374–376.
- (87) Skripov, S. E. *Nature* **2004**, *432*, 285–286.
- (88) Vidal, X.; Martorell, J. *Phys. Rev. Lett.* **2006**, *97*, 013902.
- (89) Andrews, D. L.; Allcock, P.; Demidov, A. A. *Chem. Phys.* **1995**, *190*, 1–9.
- (90) Smilowitz, L.; Henson, B. F.; Romero, J. J. *J. Phys. Chem. A* **2009**, *113*, 9650–9657.
- (91) Tammann, G.; Botschwar, A. A. *Z. Anorg. Allg. Chem.* **1926**, *157*, 27–40.
- (92) Botschwar, A. A. *Z. Anorg. Allg. Chem.* **1934**, *220*, 334–336.
- (93) Kofler, A. *J. Aust. Inst. Met.* **1965**, *10*, 132–139.
- (94) Gigliotti, M. F. X.; Colligan, G. A.; Powell, G. L. F. *Met. Trans.* **1970**, *1*, 891–897.
- (95) Coquerel, G. In *Novel Optical Resolution Technologies*; Sakai, K., Hirayama, N., Tamura, R., Eds.; Springer: Berlin, 2007; pp 1–52.
- (96) Fisher, D. J.; Kurz, W. *Acta Metall.* **1980**, *28*, 777–794.
- (97) Wanapun, D.; Kestur, U. S.; Taylor, L. S.; Simpson, G. J. *Anal. Chem.* **2011**, *83*, 4745–4751.
- (98) Kahr, B. B.; McBride, J. M. *Angew. Chem., Int. Ed. Engl.* **1992**, *31*, 1–26.
- (99) Gervais, C.; Hulliger, J. *Cryst. Growth Des.* **2007**, *7*, 1925–1935.
- (100) Vaida, M.; Shimon, L. J. W.; Weissinger-Lewin, Y.; Frolov, F.; Lahav, M.; Leiserowitz, L.; McMullan, R. K. *Science* **1988**, *241*, 1475–1479.
- (101) Shimon, L. J. W.; Vaida, M.; Frolov, F.; Lahav, M.; Leiserowitz, L.; Weissinger-Lewin, Y.; McMullan, R. K. *Faraday Discuss.* **1993**, *95*, 307.
- (102) Gervais, C.; Wüst, T.; Hulliger, J. *J. Phys. Chem. B* **2005**, *12582*–12589.
- (103) Weissbuch, I.; Lahav, M.; Leiserowitz, L.; Meredith, G. R.; Vanherzele, H. *Chem. Mater.* **1989**, *1*, 114–118.
- (104) Aboulfadl, H.; Hulliger, J. *Cryst. Growth Des.* **2011**, *11*, 3045–3048.
- (105) Rechsteiner, P.; Hulliger, J.; Flörsheimer, M. *Chem. Mater.* **2000**, *12*, 3296–3300.
- (106) Weissbuch, I.; Leiserowitz, L.; Lahav, M. *Cryst. Growth Des.* **2006**, *6*, 2–5.
- (107) Munn, R. W. *J. Chem. Phys.* **2000**, *113*, 8774.
- (108) Matsuoka, M. *Bunri Gijutsu* **1977**, *7*, 245–249.
- (109) Ulrich, J. *Cryst. Growth Des.* **2004**, *4*, 879–880.
- (110) Mahieux, J.; Sanselme, M.; Harthong, S.; Melan, C.; Aronica, C.; Guy, L.; Coquerel, G. *Cryst. Growth Des.* **2013**, *13*, 3621–3631.
- (111) Verbiest, T.; Van Elshocht, S.; Kauranen, M.; Hellmanns, L.; Snaauwaert, J.; Nuckolls, C.; Katz, T. J. *Science* **1998**, *282*, 913–915.
- (112) Busson, B.; Kauranen, M.; Nuckolls, C.; Katz, T. J.; Persoons, A. *Phys. Rev. Lett.* **2000**, *84*, 79–82.
- (113) Gervais, C.; Beilles, S.; Cardinael, P.; Petit, S.; Coquerel, G. *J. Phys. Chem. B* **2002**, *106*, 646–652.
- (114) Corvis, Y.; Négrier, P.; Massip, S.; Leger, J.-M.; Espeau, P. *CrystEngComm* **2012**, *14*, 7055–7064.
- (115) Brandel, C.; Amharar, Y.; Rollinger, J. M.; Griesser, U. J.; Cartigny, Y.; Petit, S.; Coquerel, G. *Mol. Pharmaceutics* **2013**, *10*, 3850–3861.
- (116) Amharar, Y.; Petit, S.; Sanselme, M.; Cartigny, Y.; Petit, M.-N.; Coquerel, G. *Cryst. Growth Des.* **2011**, *11*, 2453–2462.
- (117) Kurtz, S. K.; Perry, T. T. *J. Appl. Phys.* **1968**, *39*, 3798–3813.
- (118) Pawlak, D. A.; Kolodziejek, K.; Turczynski, S.; Kisielewski, J.; Roz, K.; Diduszko, R.; Kaczkan, M.; Malinowski, M. *Chem. Mater.* **2006**, *18*, 2450–2457.
- (119) Pawlak, D. A.; Kolodziejek, K.; Rozniatowski, K.; Diduszko, R.; Kaczkan, M.; Malinowski, M.; Piersa, M.; Kisielewski, J.; Lukasiewicz, T. *Cryst. Growth Des.* **2008**, *8*, 1243–1249.
- (120) Kerridge, D. H.; Horsewell, A.; Berg, R. W. *Solid State Ionics* **2009**, *180*, 1453–1456.

- (121) Pawlak, D. A.; Turczynski, S.; Gajc, M.; Kolodziejak, K.; Diduszko, R.; Rozniatowski, K.; Smalc, J.; Vendik, I. *Adv. Funct. Mater.* **2010**, *20*, 1116–1124.
- (122) Bergman, J. G. *J. Appl. Phys.* **1969**, *40*, 2860–2863.
- (123) Jackson, A. G.; Ohmer, M. C.; LeClair, S. R. *Infrared Phys. Technol.* **1997**, *38*, 233–244.
- (124) Halasyamani, P. S.; Poepelmeier, K. R. *Chem. Mater.* **1998**, *10*, 2753–2769.
- (125) Atuchin, V. V.; Kidarov, B. I.; Pervukhina, N. V. *Comput. Mater. Sci.* **2004**, *30*, 411–418.
- (126) Simon, A.; Ravez, J. C. *R. Chim.* **2006**, *9*, 1268–1276.
- (127) Chung, I.; Kanatzidis, M. G. *Chem. Mater.* **2014**, *26*, 849–869.
- (128) Porter, Y.; Ok, K. M.; Bhuvanesh, N. S. P.; Halasyamani, P. S. *Chem. Mater.* **2001**, *13*, 1910–1915.
- (129) Ok, K. M.; Bhuvanesh, N. S. P.; Halasyamani, P. S. *J. Solid State Chem.* **2001**, *161*, 57–62.
- (130) Ok, K. M.; Halasyamani, P. S. *Chem. Mater.* **2002**, *14*, 2360–2364.
- (131) Lu, H.; Gautier, R.; Donakowski, M. D.; Tran, T. T.; Edwards, B. W.; Nino, J. C.; Halasyamani, P. S.; Liu, Z.; Poepelmeier, K. R. *J. Am. Chem. Soc.* **2013**, *135*, 11942–11950.
- (132) Dityatyev, O. A.; Smidt, P.; Stefanovich, S. Y.; Lightfoot, P.; Dolgikh, V. A.; Opperman, H. *Solid State Sci.* **2004**, *6*, 915–922.
- (133) Jeong, E. D.; Borse, P. H.; Lee, J. S.; Ha, M. G.; Pak, H. K. *J. Ind. Eng. Chem.* **2006**, *12*, 790–794.
- (134) Yoon, D.-H.; Yonenaga, I.; Fukuda, T.; Ohnishi, N. *J. Cryst. Growth* **1994**, *142*, 339–343.
- (135) Yoshikawa, A.; Epelbaum, B. M.; Hasegawa, K.; Durbin, S. D.; Fukuda, T. *J. Cryst. Growth* **1999**, *205*, 305–316.
- (136) Rudolph, P.; Fukuda, T. *Cryst. Res. Technol.* **1999**, *34*, 3–40.
- (137) Goffri, S.; Müller, C.; Stingelin-Stutzmann, N.; Breiby, D. W.; Radano, C. P.; Andreasen, J. W.; Thompson, R.; Janssen, R. A. J.; Nielsen, M. M.; Smith, P.; Sirringhaus, H. *Nat. Mater.* **2006**, *5*, 950–956.
- (138) Müller, C.; Ferenczi, T. A. M.; Campoy-Quiles, M.; Frost, J. M.; Bradley, D. D. C.; Smith, P.; Stingelin-Stutzmann, N.; Nelson, J. *Adv. Mater.* **2008**, *20*, 3510–3515.
- (139) Smith, J.; Hamilton, R.; McCulloch, I.; Stingelin-Stutzmann, N.; Heeney, M.; Bradley, D. D. C.; Anthopoulos, T. D. *J. Mater. Chem.* **2010**, *20*, 2562.
- (140) Zheludev, N. I. *Science* **2010**, *328*, 582–583.
- (141) Lapine, M.; Shadrivov, I. V.; Kivshar, Y. S. *Rev. Mod. Phys.* **2014**, *86*, 1093–1123.
- (142) Valev, V. K.; Baumberg, J. J.; Sibilia, C.; Verbiest, T. *Adv. Mater.* **2013**, *25*, 2517–2534.
- (143) Martorell, J.; Vilaseca, R.; Corbalán, R. *Appl. Phys. Lett.* **1997**, *70*, 702.
- (144) Berger, V. *Phys. Rev. Lett.* **1998**, *84*, 4136–4139.
- (145) Demeyer, P.; Vandendriessche, S.; Van Cleuvenbergen, S.; Carron, S.; Bogaerts, K.; Parac-Vogt, T. N.; Verbiest, T.; Clays, K. *ACS Appl. Mater. Interfaces* **2014**, *6*, 3870–3878.
- (146) Pawlak, D. A. *Sci. Plena* **2008**, *4*, 014801.